Geochemistry, U-Pb SHRIMP zircon dating and Hf isotopes of the Gondwanan magmatism in NW Argentina: petrogenesis and geodynamic implications

Stella Poma[1], Eduardo O. Zappettini[2], Sonia Quenardelle[1], João O. Santos[3], †Magdalena Koukharsky[1], Elena Belousova[4], Neil McNaughton[3]

[1] *Instituto de Geociencias Básicas, Aplicadas y Ambientales de Buenos Aires (IGEBA-CONICET), Universidad de Buenos Aires, Facultad de Ciencias Exactas y Naturales, Departamento de Ciencias Geológicas, Pabellón II-Ciudad Universitaria, Intendente Güiraldes 2160, C1428 EGA, Argentina.*
stella@gl.fcen.uba.ar; sonia@gl.fcen.uba.ar

[2] *Servicio Geológico Minero Argentino (SEGEMAR), Avda. General Paz 5445, edificio 25, San Martín B1650WAB, Argentina.*
eduardo.zappettini@segemar.gov.ar

[3] *University of Western Australia, 35 Stirling Highway, Crawley WA 6009, Australia.*
orestes.santos@bigpond.com; N.Mcnaughton@curtin.edu.au

[4] *ARC National Key Centre for Geochemical Evolution and Metallogeny of Continents (GEMOC), Macquarie University, Sydney NSW 2109, Australia.*
ebelouso@els.mq.edu.au

ABSTRACT. We have carried out zircon U-Pb SHRIMP dating and Hf isotope determinations as well as geochemical analyses on three plutonic units of Gondwanan magmatism that crop out in NW Argentina. Two episodes of different age and genesis have been identified. The older one includes gabbros and diorites (Río Grande Unit) of 267±3 Ma and granitoids (belonging to the Llullaillaco Unit) of 263±1 Ma (late Permian, Guadalupian); the parent magmas were generated in an intraplate environment and derived from an enriched mantle but were subsequently contaminated by crustal components. The younger rocks are granodiorites with arc signature (Chuculaqui Unit) and an age of 247±2 Ma (middle Triassic-Anisian). Hf isotope signature of the units indicates mantle sources as well as crustal components. Hf model ages obtained are consistent with the presence of crustal Mesoproterozoic (mainly Ectasian to Calymnian ($T_{DM(c)}$=1.24 to 1.44 Ga-negative $_{Hf(T)}$) and juvenile Cryogenian sources (T_{DM}=0.65 to 0.79 Ga-positive $\varepsilon_{Hf(T)}$), supporting the idea of a continuous, mostly Mesoproterozoic, basement under the Central Andes, as an extension of the Arequipa-Antofalla massif. The tectonic setting and age of the Gondwanan magmatism in NW Argentina allow to differentiate: **a.** Permian intra-plate magmatism developed under similar conditions to the upper section of the Choiyoi magmatism exposed in the Frontal Cordillera and San Rafael Block, Argentina; **b.** Triassic magmatism belonging to a poorly known subduction-related magmatic arc segment of mostly NS trend with evidence of porphyry type mineralization in Chile, allowing to extend this metallotect into Argentina.

Keywords: Gondwanan magmatism, Geochemistry, U-Pb SHRIMP dating, Lu-Hf isotope, NW Argentina.

RESUMEN. Geoquímica, dataciones U-Pb SHRIMP sobre circón e isótopos de Hf del magmatismo gondwánico en el NW de Argentina: petrogénesis e implicancias geodinámicas. Se presentan resultados de la geoquímica, dataciones U-Pb SHRIMP y de relaciones isotópicas Lu-Hf de tres unidades plutónicas pertenecientes al magmatismo gondwánico del NW de Argentina. Se identificaron dos episodios de diferente edad y génesis. El más antiguo incluye gabros y dioritas (Unidad Río Grande) de edad 267±3 Ma y granitoides (pertenecientes a la Unidad Llullaillaco) de 263±1 Ma (Pérmico tardío-Guadalupiense) generados en un ambiente de intraplaca a partir de un manto enriquecido y subsecuentemente contaminado con componentes corticales. El evento más joven está representado por la intrusión de granodioritas (Unidad Chuculaqui) de 247±1 Ma (Triásico medio-Anisiense) con características químicas de arco magmático. El comportamiento de los isótopos de Hf de las unidades estudiadas indica la participación de fuentes mantélicas como así también de componentes corticales en su generación. Las edades modelo Hf obtenidas son consistentes con la presencia de fuentes corticales del Mesoproterozoico (principalmente Ectasiano a Calimniano (1,24 a 1,44 Ga-$\varepsilon_{Hf(T)}$ negativo) y juveniles del Criogeniano (T_{DM}=0,65 to 0,79 Ga-$\varepsilon_{Hf(T)}$ positivo), lo que está de acuerdo con la presencia de un basamento continuo, de ese rango de edades, bajo los Andes Centrales, como una extensión del macizo de Arequipa-Antofalla. El ambiente tectónico y la edad del magmatismo gondwánico en el NW de Argentina permiten diferenciar: **a.** Un magmatismo pérmico de intraplaca desarrollado bajo condiciones similares a las del magmatismo carbonífero de intraplaca descrito para Cordillera Frontal y Bloque de San Rafael; **b.** Un magmatismo triásico perteneciente a un segmento de arco magmático de orientación predominante NS con evidencias de mineralización tipo pórfiro en Chile, lo que permite extender este metalotecto en el territorio argentino.

Palabras clave: Magmatismo gondwánico, Geoquímica, Dataciones U-Pb SHRIMP, Isotopía Lu-Hf, NW Argentina.

1. Introduction

A long and discontinuous Permian/Triassic magmatic belt occurs along the western margin of Gondwana in South America, outcropping from central Perú as far as approximately 39ºS in Argentina. From west to east it extends approximately 600 km from the Gondwana margin into the foreland, reaching the longitude of the present Sierras Pampeanas and the western margin of the Río de la Plata craton (Fig. 1, inset). It comprises epizonal plutonic and volcanic rocks, the latter including pyroclastic facies. In Argentina and Chile the assemblage has been named Choiyoi magmatic province (Kay *et al*., 1989; Llambías *et al*., 1993; Llambías, 1999), even though originally the term Choiyoi was used to identify only the volcanic units (originally Groeber, 1946, 1951, and later Choiyoi Group; *e.g*., Llambías *et al*., 1993).

In Argentina, the Choiyoi igneous rocks crop out in the basement of the Neuquén basin and the main Cordillera of southern Mendoza, in the Cordillera Frontal of Mendoza and San Juan, San Rafael block and its southern extension in the La Pampa province. To the NW the magmatic province extends into Chile and to the SE into northern Patagonia. The Cordillera Frontal outcrops are the most voluminous and have been the subject of study over the last 40 years (*e.g.,* Rolleri and Criado Roque, 1970; Mpodozis and Kay, 1992; Llambías *et al.,* 1993, Breitkreuz and Zeil, 1994; Lucassen *et al*., 1999). This region is characterized by felsic rocks with subordinated basic and mesosilicic rocks. Volcanic sequences dominate in Argentina and plutonic rocks in Chile, although important plutons such as the Colangüil Batholith also occur in Argentina (Llambías and Sato, 1990, 1995).

Isolated Permian-Triassic plutons have been recognized in the Puna region of Salta province, Argentina, suggesting that the magmatic event reached that latitude (Zappettini and Blasco, 1998; Page and Zappettini, 1999; Poma *et al*., 2009).

The aim of this paper is to contribute to the knowledge of the Gondwanan magmatism through the presentation and interpretation of chemical and isotopic data of previously poorly known units that represent the northernmost outcrops identified in Argentina. We present new zircon U-Pb SHRIMP and Hf isotope data and we explore the nature and characteristics of the magma sources to better constrain a petrogenetic model and characterize the crustal components of the Puna region.

2. Geological setting

The basement of the western margin of Gondwana consists of several terranes amalgamated against the Río de la Plata and the Amazonas cratons. It includes the Antofalla-Arequipa, Pampia, Cuyania and Chilenia terranes that are thought to have accreted from Late Neoproterozoic to Devonian times (Ramos *et al*., 2010 and references therein). Records of subduction and related arc magmatism
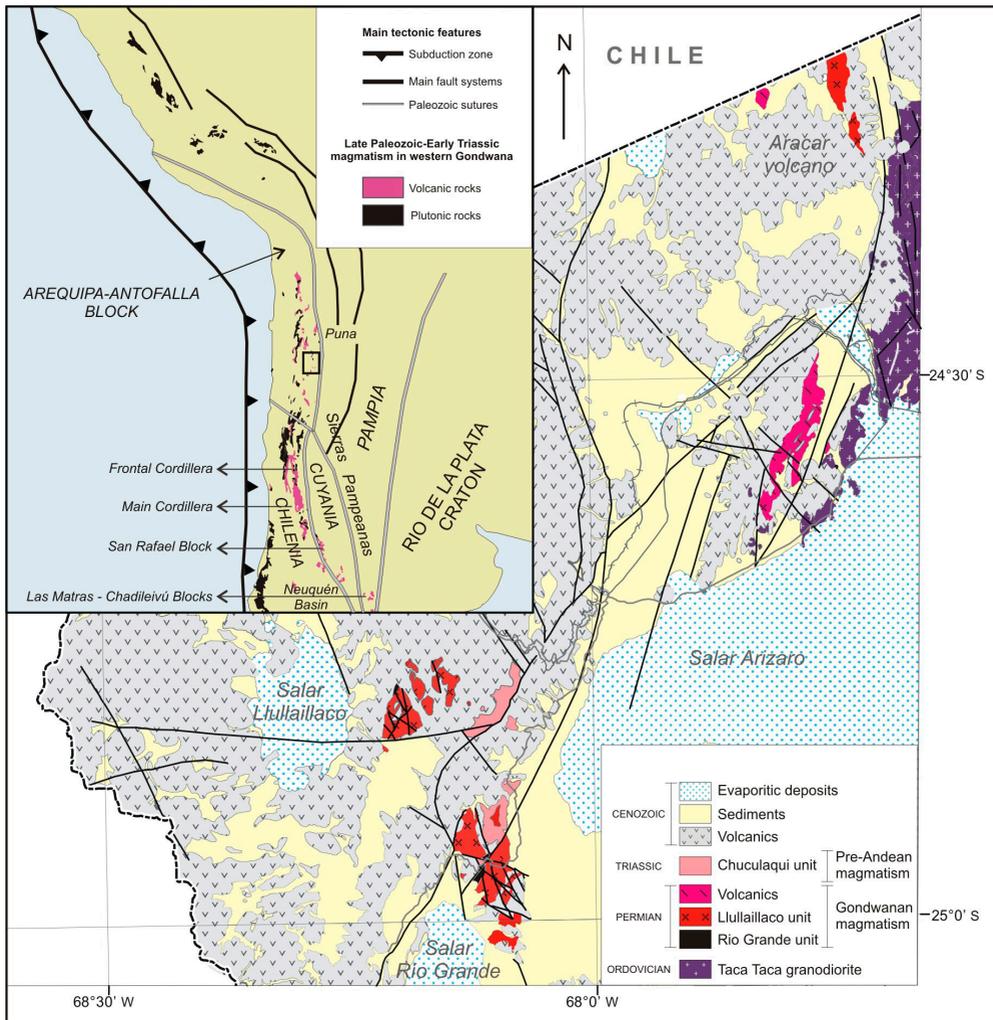
FIG. 1. The Gondwanan magmatism in the Socompa region. Inset: distribution of the late Paleozoic-Early Triassic magmatism in South America. Main tectonic features are also indicated.

in the western margin of Gondwana are almost continuous during the Phanerozoic, although there is evidence for a time of relative quiescence during the Devonian and Early Mississippian (390 to 340 Ma) from northern Perú to southern Chile due to the development of a passive margin at those times (Bahlburg *et al.*, 2009). In central to southern Chile this scenario is related to the prior collision of Chilenia (Willner *et al.*, 2009).

In NW Argentina the first records of magmatism are related to the Pampean and Famatinian orogenies (Rapela *et al.*, 1998; Pankhurst *et al.*, 1998). The Pampean magmatism is restricted to the Eastern Cordillera (Cañani, La Quesera and Chañi

units) (Omarini *et al.*, 2008) and the Famatinian magmatism (Bahlburg *et al.*, 2009) includes both the Faja Eruptiva de la Puna Occidental magmatic arc (Poma *et al.*, 2004) and the Faja Eruptiva de la Puna Oriental back-arc magmatism (Coira, 2008; Zappettini, 2008).

During the early Carboniferous magmatism was reinitiated along the Gondwana margin in the central and southern Andes (Kay *et al.*, 1989; Brown, 1991; Breitkreuz *et al.*, 1992; Breitkreuz and Van Schmus, 1996). In particular, intrusive activity began around 330 Ma (Lucassen *et al.*, 1999 and references therein). I-type earliest subduction-related granitoids are recorded in the Eastern Cordillera

of Perú with U-Pb zircon ages at *ca.* 350-325 Ma (Miskovic *et al.*, 2009), between 21° and 22°S in Chile (Ujina, Rosario, El Colorado and Quebrada Blanca porphyries, Collahuasi Group, 300 Ma; cf. Munizaga *et al.*, 2008) and between 28° and 29°S in Argentina (*e.g.*, Tabaquito pluton, 326-329 Ma; Los Guandacolinos Granite, 314 Ma; Cerro Veladero Granite, 311 Ma; Cerro de las Tunas, 330 Ma; cf. Alasino *et al.*, 2012).

A subduction-related setting has been also ascribed to Permian magmatism and Triassic units have been interpreted to be the result of partial rifting and trans-tension following the suture of the Arequipa-Antofalla terrane and the Amazonian craton, due to stresses originated during the Pangea break-up (Kontak *et al.*, 1990; Atherton and Petford, 1990). Although, other authors have pointed out that an early stage the magmatism was related to subduction, followed by non orogenic magmatism related to active rifting (Kay *et al.*, 1989; Mpodozis and Ramos, 1990; Llambías and Sato, 1990). Kleiman and Japas (2009) and Rocha Campos *et al.* (2011) consider that the 31°S to 36°S segment could be regarded as a transitional zone between different subduction segments after 270 Ma. The northern segment would be normal in dip angle and the southern shallower of that. It should be noted that in northern Chile, there is evidence of arc-related magmatism of Triassic age with porphyry copper-related mineralization (243.2±2.1 to 248.7±3.3 Ma U-Pb SHRIMP; Munizaga *et al.*, 2008).

In the Puna region of Argentina, the Gondwanan magmatism is represented by both plutonic and volcanic rocks that extend along a discontinuous NNE-SSW belt from 24° to 26°S. Andean tectonics have affected the continuity of this belt and Cenozoic volcanism covers most of the region. Late Paleozoic outcrops include the León Muerto Granite (25°48'S /68°24'W), a porphyritic amphibole granite (Page y Zappettini, 1999) dated at 246±6 Ma (K-Ar whole rock; Naranjo and Cornejo, 1992); Ojo de Antofalla Granite (25°26'19"S/67°39'05"W) and a subvolcanic pluton dated at 235±10 Ma (K-Ar whole rock; Martos, 1981[1]). Northward the Llullaillaco plutonic complex (Zappettini and Blasco, 1998), herein described as Llullaillaco Unit, include outcrops between 24°10'S and 25°S (NE of Aracar volcano, N of Taca-Taca

Range, NW of Agua del Desierto, SW of Pie de Samenta, NE of Salar Río Grande, East of Salar de Llullaillaco). It comprises porhyritic rocks, dated at 257±18 Ma (K-Ar whole rock) and a red granite with a K-Ar (biotite) age of 224±5 Ma. One red granite that crops out to the west of Incahuasi Salar yielded 266±1 Ma and one microgranitoid was dated at 269±2 Ma (conventional U-Pb on zircon; Page and Zappettini, 1999). This complex is correlated with the intrusive bodies known as Plutones Guanaqueros (282±7 Ma; Gardeweg *et al.*, 1993).

Associated volcanic rocks have been identified to the north of the Aracar volcano, named as the Laguna de Aracar Formation (Koukharsky, 1969[2]) that extends southward along the NW border of the Arizaro Salar. It comprises acidic volcanic and pyroclastic rocks dated at 266±28 Ma (K-Ar whole rock; Zappettini and Blasco, 1998). Equivalent volcanic sequences in Chile have been dated at 259±8 Ma and 261±9 Ma (K-Ar whole rock; Ramírez *et al.*, 1991).

Other plutonic outcrops of the region have been assigned to the Gondwanan magmatism as an outcome of the mapping and geochronological studies herein presented. They are herein identified as Río Grande and Chuculaqui Units and were originally assigned to the Famatianian magmatic arc (Zappettini and Blasco, 1998).

We have focused the work on the description of the Río Grande, Llullaillaco and Chuculaqui Units (Fig. 1).

The Río Grande Unit form small outcrops to the East of the Llullaillaco salar and also to the north of the Río Grande salar where it is intruded by the Chuculaqui granitoids. These rocks intrude Ordovician metasediments unit (Zappettini and Blasco, 1998).

The Llullaillaco Unit constitutes three main groups of outcrops located to the NE of the Aracar volcano, to the East of the Llullaillaco salar and to the North of the Río Grande salar. Outcrops are partially covered by Cenozoic lava flows and intrude rocks of the Río Grande Unit (Zappettini and Blasco, 1998).

The Chuculaqui Unit is located to the West in the center south extreme of the studied region. It constitutes two main bodies and minor satellital outcrops partially cover by the Cenozoic volcanites.

---

[1] Martos, D. 1981. Estudio geológico económico del sector sudeste del área de reserva N°5 'Antofalla Este'. Facultad de Ciencias Naturales UNT (Unpublished): 83 p. Tucumán.

[2] Koukharsky, M. 1969. Informe preliminar sobre la estratigrafía de la Hoja 6ª Socompa, Provincia de Salta. Instituto Nacional de Geología y Minería (Unpublished): 22 p. Buenos Aires.

The Chuculaqui rocks intrude red granites asigned to the Llullaillaco Unit (Zappettini and Blasco, 1998).

3. Petrography

3.1. Río Grande Unit

This unit includes gabbros, diabases and diorites with hypidiomorphic granular to porphyritic texture, sometimes exhibiting igneous lamination, as it is frequently displayed by plagioclase feldspar. The most abundant minerals are plagioclase, pyroxene and olivine. Plagioclase crystals are zoned, locally showing patchy extinction due to complex zoning patterns and variable Ca-Na compositions, these being characteristics compatible with mixing-mingling processes; labradorite-bytownite has been recognized in the basic varieties, and andesine-oligoclase in the mesosilicic types. Ortho- and clino-pyroxene are replaced by fibrous amphibole pseudomorphs with a few crystals showing preserved cores. Olivine is present in a few samples showing partial replacement by an orthopyroxene rim. Accessory minerals include apatite (0.5 to 5.4 mm in length), sphene, zircon and opaque minerals; some are euhedral but there is a predominance of rounded shapes like drops. Locally, plagioclase cumulate textures have been recognized.

3.2. Llullaillaco Unit

It consists of red granite, with subordinated microdioritic facies. The main facies is a leucocratic reddish alkali-feldspar granite. The textures are granular and microgranular allotriomorphic, with simultaneous growth of alkali feldspars and quartz producing granophyre intergrowth; miarolitic structures are also observed. These textures indicate rapid cooling conditions and shallow emplacement. Quartz crystals usually have rounded borders although some of them show original bipyramidal habit. Alkali feldspar is strongly perthitic and plagioclase is scarce or not visible. Biotite is subordinated (about 1%) and it is frequently replaced by chlorite and epidote. Accessory minerals are zircon, apatite needles, fluorite forming mosaic crystals grouped in cavities (upholster vugs without evidence of lined), and rounded grains of magnetite. The presence of one alkali perthitic feldspar is compatible with an hypersolvus granite (Bowen and Tuttle, 1950; Tuttle and Bowen, 1958).

3.3. Chuculaqui Unit

This unit comprises gray tonalites to granodiorites as the main facies, with subordinate granites and quartz-diorites. Poma *et al.* (2009) described associated mafic facies in the borders of this plutonic suite, including gabbroid lenses like mafic microgranular enclaves. These are microdioritic in composition and the material is hybridized in various degrees. Field relationships indicate that during emplacement the silicic melt incorporated mafic material; additional textural evidence indicates in some localities that the granitic intrusion was probably coeval with the mafic magmatism.

The rocks are hypidiomorphic, with inequigranular medium to coarse grains. In some granitic rocks monzonitic textures are common showing poikilitic quartz and K-feldspar enclose euhedral plagioclase and prismatic amphibole.

The most abundant mineral is zoned oligoclase (An_{26-28}) with light sericitic alteration; alkali feldspar crystals (orthoclase) are perthitic. In the granodiorite facies, plagioclase occasionally shows a myrmekitic intergrowth at grain boundaries with alkali feldspar. The mafic minerals (10% to 20%) are amphibole and scarce biotite, both of them partially replaced by epidote, chlorite and associated opaque minerals. Accessory minerals are idiomorphic sphene, apatite, zircon and opaque minerals.

4. Geochemistry

The studied units cover a wide compositional range (Fig 2a, Table 1) from gabbros (45% SiO_2) to high silica granites (up to 78% SiO_2). In the K_2O *versus* SiO_2 diagram (Fig. 2b) the Río Grande Unit rocks plot in the medium- to high-K field, the Llullaillaco Unit is constrained to the high-K field and Chuqulaqui Unit spans the medium- and high-K fields.

The Río Grande Unit gabbros and diorites are metaluminous subalkaline basic to mesosilic rocks with high values of FeO, CaO and MgO, and variable contents of Na_2O and Ti_2O. Zr shows a positive correlation with SiO_2. In the MORB-normalized trace element spider diagrams (Pearce, 1983) the rocks (Fig. 3a) display a continuous variation in HFSE contents, in particular Nb, Ta, Zr, Hf and Ti depletion. The REE diagram (Fig. 4a) is characterized by a relatively low La/Yb slope and Eu
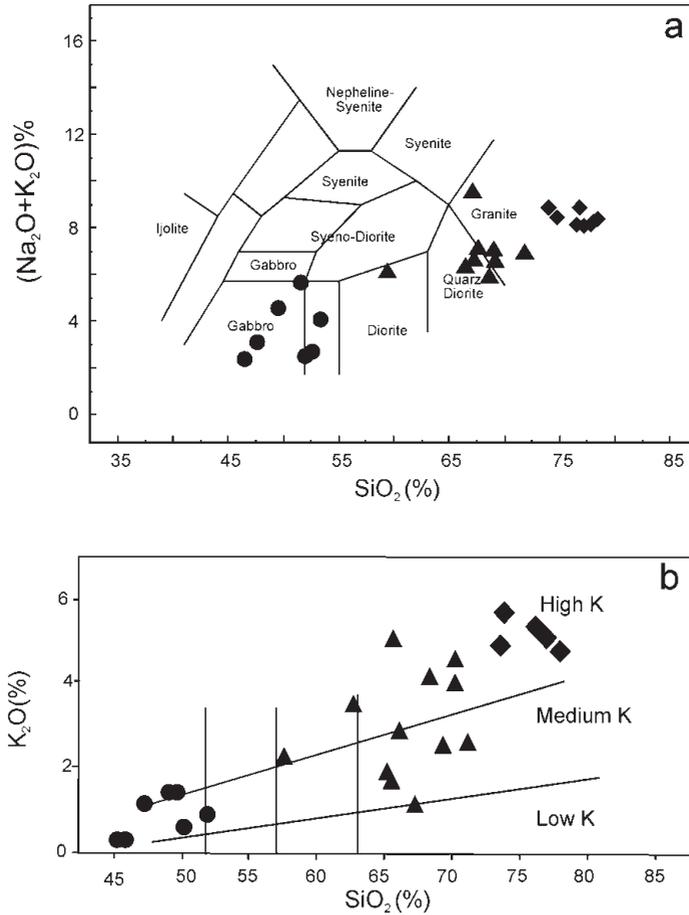
FIG. 2. **a.** TAS plutonic classification by Cox *et al.* (1979); **b.** K$_2$O *versus* SiO$_2$ plot (Peccerillo and Taylor, 1976). **Diamond:** Llullaillaco Unit, **Circles:** Río Grande Unit, **Triangles:** Chuculaqui Unit.

anomalies (0.81 to 1.42) coincident with the presence of cumular plagioclase as was petrographically identified.

The red granites of the Llullaillaco Unit have characteristics of evolved high-silica magma with low FeO, MgO, CaO contents and are slightly peraluminous with A/CNK ≤1.1 (Table 1). A distinguishing characteristic is their high Rb, Th and U contents and low Sr. Zircon contents show a random distribution *versus* SiO$_2$. The discrimination diagram of Pearce (1984) shows (Fig. 5a) the granitoids plot in volcanic arc field transitional to the within plate field. In a spider diagram normalized to MORB (Fig. 3b) rocks show a consistent pattern characterized by strong depletion in Ba and Ce, and high Th. The REE diagram (Fig. 4b) is characterized by having a sharp negative Eu anomaly related to plagioclase

fractionation and low La/Yb ratio suggesting the presence of a low-pressure residual mineralogy in the source.

The Chuculaqui Unit rocks span between 65 and 70% SiO$_2$ and are metaluminous, plotting in the VAG field (Fig. 5a). These rocks have characteristically variable La/Ta ratios even higher than 30 and Ba/Ta ratios (Fig. 5b) greater than 450. Zr values decrease with increasing SiO$_2$ indicating a normal negative trend. In a MORB-normalized spider diagram (Fig. 3c) all samples exhibit enriched LILE (Ba) relative to light REE and both enriched relative to HFSE Nb, Ta, Zr, and Hf, corresponding to continental arc-related signatures. The REE diagrams (Fig. 4c) show small negative anomalies in Eu (0.66 to 0.93) indicative of plagioclase fractionation and La/Yb ratios <9.

TABLE 1. GEOCHEMICAL DATA.

	Río Grande Unit							Llullaillaco Unit								Chuqulaqui Unit								
	SA 02/03	SA 06/03	SA 07/03	SA 08/03	SA 09/03	RioG1	RioG2	SA 10/03	M00/72	M643	M634	M30	M644	M665	M664	Chuq	SA 12/03	SA 05/03	SA 01/03	M00/60	M00/63	M00/69	M00/71	M637
SiO_2	49.44	51.70	45.16	45.54	47.60	49.25	50.48	77.98	75.94	77.99	78.00	77.05	73.86	75.96	73.63	68.60	65.88	57.66	67.18	65.67	65.63	70.05	68.38	65.42
TiO_2	1.55	1.05	0.83	1.51	1.63	2.72	2.50	0.12	0.20	0.13	0.10	0.08	0.26	0.16	0.58	0.40	0.61	1.23	0.37	0.42	0.48	0.37	0.48	0.49
$Al2O_3$	18.46	15.27	21.09	19.35	17.67	15.50	16.10	11.31	12.41	11.64	12.50	12.22	13.38	12.23	12.32	16.09	14.89	16.00	16.33	16.09	16.58	14.01	14.75	15.14
Fe_2O_3	9.21	8.99	9.94	9.52	10.72	11.82	10.05	1.24	2.06	1.13	0.88	1.60	2.44	1.17	3.11	3.02	4.25	7.22	3.23	3.67	3.67	3.11	3.99	5.08
MnO	0.12	0.17	0.11	0.14	0.16	0.22	0.25	0.01	0.02	0.03	0.02	0.02	0.05	0.05	0.03	0.06	0.07	0.13	0.05	0.06	0.06	0.08	0.09	0.03
MgO	4.38	6.82	6.69	6.55	5.07	4.52	4.22	0.05	0.13	0.07	0.06	0.07	0.36	0.01	0.01	1.34	2.11	3.42	1.09	1.52	1.63	0.93	1.21	1.35
CaO	7.62	9.19	11.86	10.43	9.11	7.24	7.80	0.38	0.39	0.64	0.49	0.41	0.79	0.88	0.58	3.67	2.92	6.00	4.12	3.98	4.41	2.30	3.02	0.86
Na_2O	3.82	2.94	1.99	2.62	3.24	4.22	5.02	3.55	2.81	3.51	3.38	3.87	3.24	2.69	3.35	4.42	3.89	3.73	4.72	4.39	4.44	2.82	2.84	4.44
K_2O	1.55	0.96	0.26	0.33	1.11	1.39	0.62	4.73	5.23	4.67	4.75	4.96	5.55	5.23	4.90	1.99	2.79	2.13	1.10	1.87	1.68	3.92	3.92	4.89
P_2O_5	0.57	0.56	0.10	0.52	0.78	1.04	1.06	0.02	0.05	0.02	0.02	0.06	0.08	0.05	0.22	0.12	0.16	0.47	0.15	0.14	0.15	0.09	0.63	0.23
LOI	2.44	1.57	0.83	2.24	1.53	2.11	1.92	0.46	0.80	n.d.	n.d.	n.d.	n.d.	n.d.	n.d.	1.18	1.54	1.28	1.25	0.87	0.89	1.57	0.86	n.d.
A/CNK	0.85	0.68	0.84	0.82	0.77	0.72	0.70	0.97	1.13	0.97	1.08	0.98	1.05	1.05	1.04	1.00	1.01	0.83	0.99	0.98	0.97	1.07	1.02	1.07
La	24.70	34.30	9.87	14.10	35.60	35.00	39.00	28.10	28.90	30.30	15.50	43.70	36.20	20.60	40.60	17.90	33.30	46.00	11.80	18.80	18.50	33.20	34.30	35.00
Ce	54.40	74.50	19.80	32.30	78.90	77.40	91.00	64.70	55.60	74.30	48.80	119.00	106.00	42.00	84.00	34.50	67.90	98.00	24.70	36.60	37.40	61.50	65.60	79.70
Pr	7.14	9.71	2.47	4.61	10.40	9.98	11.20	8.10	5.46	9.28	3.85	11.73	8.05	0.10	0.10	3.72	8.19	12.30	3.06	3.88	4.19	6.06	6.53	7.78
Nd	29.50	38.60	9.85	21.10	42.10	41.20	46.10	33.50	18.60	38.90	14.30	43.40	29.00	15.00	39.00	13.60	29.90	48.30	12.00	15.60	16.60	21.80	24.40	29.00
Sm	6.27	8.39	2.15	4.63	8.88	8.40	9.00	8.12	3.42	10.90	3.03	10.40	5.64	3.10	6.90	2.60	6.01	9.81	2.53	2.91	3.31	3.65	4.31	5.15
Eu	2.01	2.02	0.91	1.70	2.25	2.04	2.32	0.43	0.52	0.51	0.32	0.27	1.03	0.80	1.40	0.69	1.21	2.23	0.74	0.80	0.92	0.94	1.07	1.21
Gd	5.33	7.01	1.79	4.08	7.44	7.30	7.90	8.12	3.52	10.60	2.45	9.30	4.44	0.10	0.10	2.40	4.85	8.02	2.23	2.79	3.09	3.59	4.60	3.70
Tb	0.74	1.07	0.27	0.53	1.08	1.10	1.10	1.53	0.56	2.07	0.50	1.95	0.79	0.70	0.90	0.40	0.81	1.23	0.32	0.38	0.43	0.49	0.65	0.62
Dy	3.98	5.72	1.44	2.64	5.52	5.50	6.00	10.10	3.60	13.00	3.03	11.90	4.53	0.10	0.10	2.20	4.36	6.30	1.68	2.16	2.40	2.84	3.78	3.29
Ho	0.76	1.16	0.28	0.49	1.06	1.10	1.10	2.19	0.79	2.68	0.68	2.48	0.91	0.10	0.10	0.40	0.89	1.22	0.32	0.41	0.47	0.59	0.79	0.61
Er	2.10	3.31	0.77	1.28	3.01	2.80	2.90	6.77	2.69	7.60	2.26	7.53	2.75	0.10	0.10	1.10	2.69	3.58	0.94	1.23	1.38	1.83	2.37	1.78
Tm	0.28	0.48	0.11	0.16	0.42	0.38	0.42	1.05	0.46	1.24	0.43	1.28	0.44	0.10	0.10	0.18	0.41	0.52	0.14	0.19	0.20	0.29	0.37	0.25
Yb	1.73	2.92	0.69	0.88	2.45	2.40	2.50	6.66	3.27	7.67	3.05	7.97	2.91	0.10	0.10	1.20	2.68	3.13	0.91	1.22	1.39	2.01	2.43	1.58
Lu	0.24	0.41	0.10	0.11	0.34	0.33	0.34	0.92	0.55	1.07	0.50	1.16	0.43	0.10	0.10	0.17	0.39	0.46	0.13	0.18	0.20	0.31	0.38	0.24
Sr	730.00	585.00	765.00	804.00	728.00	564.00	666.00	11.00	44.00	17.00	21.00	18.00	181.00	95.00	122.00	419.00	360.00	523.00	530.00	436.00	498.00	138.00	164.00	168.00
Ba	368.00	475.00	175.00	256.00	434.00	141.00	146.00	17.00	349.00	67.00	37.00	205.00	867.00	690.00	908.00	376.00	698.00	586.00	274.00	415.00	755.00	578.00	475.00	1205.00
Cs	9.00	0.70	1.00	1.10	0.90	4.30	1.70	1.00	7.60	1.20	9.70	1.30	5.90	5.00	2.50	1.20	2.20	3.80	0.60	8.00	1.40	9.70	7.90	0.90
U	1.08	1.89	0.34	0.16	1.46	1.30	1.20	3.95	3.24	n.d.	n.d.	n.d.	n.d.	n.d.	n.d.	1.60	2.51	2.92	0.76	1.43	1.06	2.47	2.57	n.d.
Th	4.78	9.11	1.49	0.59	6.63	5.10	5.90	24.70	28.20	25.60	50.90	27.50	40.00	11.20	16.30	5.90	14.60	15.20	2.34	6.56	6.14	13.90	14.50	9.82
Hf	2.50	4.20	1.10	0.50	3.30	3.80	3.80	7.60	3.80	7.00	2.40	7.50	6.70	3.00	5.90	2.60	5.70	6.90	3.40	3.30	3.40	3.90	4.50	5.00
Ta	1.90	0.47	0.11	0.05	0.45	0.70	0.80	2.63	2.06	2.56	1.79	2.53	2.02	0.90	1.00	0.70	0.93	1.01	0.25	0.43	0.45	0.92	1.00	1.04
Sc	18.00	27.00	15.00	18.00	21.00	33.00	29.00	3.00	4.00	3.00	2.00	2.00	5.00	3.00	6.00	6.00	10.00	16.00	4.00	8.00	8.00	8.00	11.00	6.00
Cr	40.00	280.00	150.00	60.00	50.00	15.00	15.00	<20	<20	20.00	<20	<20	<20	0.10	7.00	15.00	20.00	40.00	<20	<20	<20	<20	<20	<20
Ni	50.00	80.00	150.00	60.00	270.00	40.00	40.00	<20	<20	n.d.	n.d.	n.d.	n.d.	n.d.	n.d.	15.00	<20	30.00	<20	<20	<20	<20	<20	n.d.
Co	30.00	32.00	46.00	36.00	35.00	52.00	34.00	<1	2.00	n.d.	n.d.	n.d.	n.d.	n.d.	n.d.	36.00	11.00	19.00	3.00	8.00	7.00	7.00	8.00	n.d.
Rb	87.00	34.00	7.00	11.00	34.00	80.00	33.00	256.00	221.00	235.00	219.00	240.00	261.00	166.00	177.00	50.00	87.00	77.00	33.00	43.00	149.00	149.00	152.00	154.00
Nb	10.90	6.90	1.90	0.60	6.00	11.00	12.00	35.70	9.70	35.00	13.00	42.00	22.00	0.10	0.10	5.00	12.10	15.20	4.00	3.10	5.50	5.50	6.80	16.00
Zr	85.00	163.00	38.00	11.00	113.00	152.00	162.00	169.00	107.00	150.00	50.00	164.00	198.00	74.00	238.00	101.00	203.00	264.00	117.00	119.00	123.00	143.00	161.00	163.00
Y	22.40	33.20	8.30	14.10	30.70	28.00	29.00	65.80	23.50	n.d.	n.d.	n.d.	n.d.	n.d.	n.d.	11.00	27.90	37.60	10.10	10.00	12.00	17.50	23.20	n.d.
Latitude-S	24° 52' 31.8"	24° 52' 40.3"	24° 52' 24.8"	24° 53' 18.4"	24° 52' 34.3"	24° 56' 30.6"	24° 56' 30.6"	24° 52' 24.9"	24° 37' 50.3"	24° 57' 05.5"	24° 45' 44.0"	24° 18' 06.9"	24° 57' 07.4"	24° 46' 11.5"	24° 46' 11.4"	24°49' 04.5"	24° 52' 12.8"	24° 52' 16.5"	24° 54' 14.7"	24° 49' 15.5"	24° 49' 15.5"	24° 37' 48.2"	24° 37' 23.8"	24° 55' 20.6"
Longitude-W	68° 05' 55.5"	68° 06' 21.3"	68° 05' 49.3"	68° 06' 26.1"	68° 06' 33.0"	68° 06' 38.9"	68° 06' 38.9"	68° 05' 45.1"	67° 45' 24.5"	68° 06' 48.0"	68° 09' 23.3"	67° 42' 31.5"	68° 06' 50.8"	68° 11' 05.5"	68° 11' 05.5"	68° 06' 01.0"	68° 05' 39.7"	68° 05' 40.0"	68° 05' 02.4"	68° 05' 54.3"	68° 05' 54.3"	67° 45' 41.4"	67° 45' 19.4"	68° 05' 42.0"
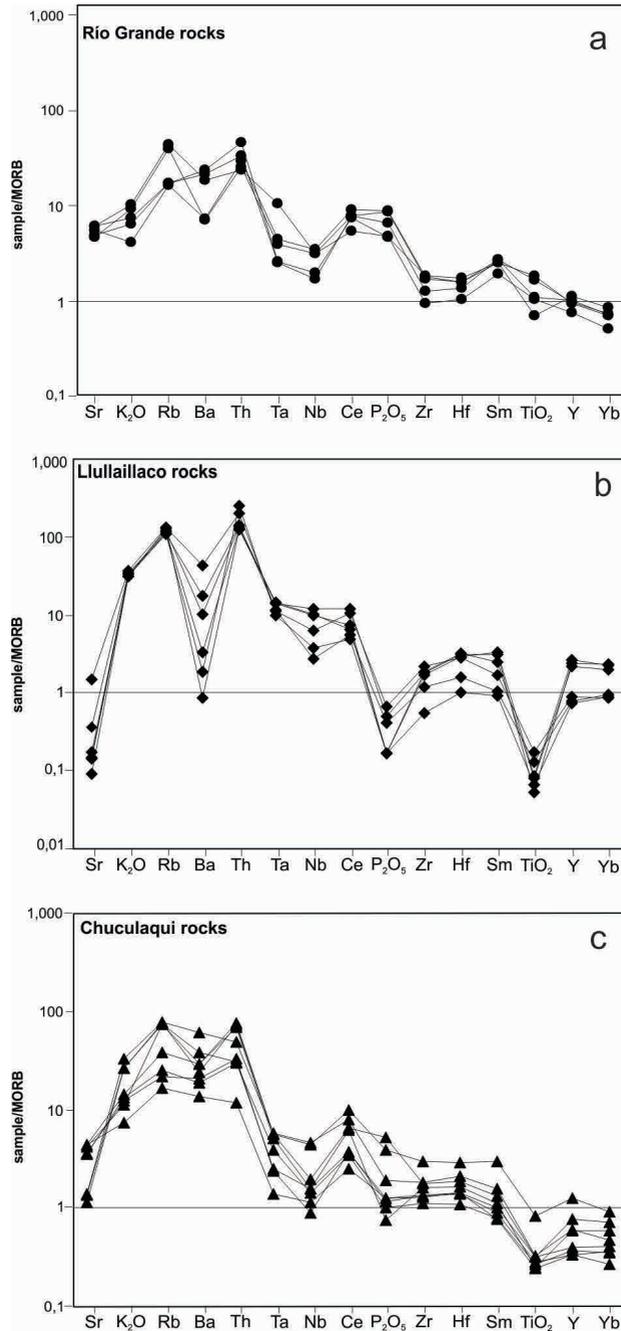
FIG. 3. MORB normalized spider diagrams following Pearce (1983). **a.** Río Grande; **b.** Llullaillaco; **c.** Chuculaqui rock samples. Symbols same as figure 2.

5. U-Pb and Lu-Hf systematics

Zircons were separated from representative samples of the Río Grande (RG: 24°56'30.61''S-68°06'38.88''W), Llullaillaco (SA10-03: 24°52'24.9''S -68°05'45.10''W) and Chuculaqui (CHUQ: 24°49'4.53''S-68°06'1.04''W) units. A full description of the samples preparation and analytical methods is presented in Appendix. Only relevant information is given in this chapter.
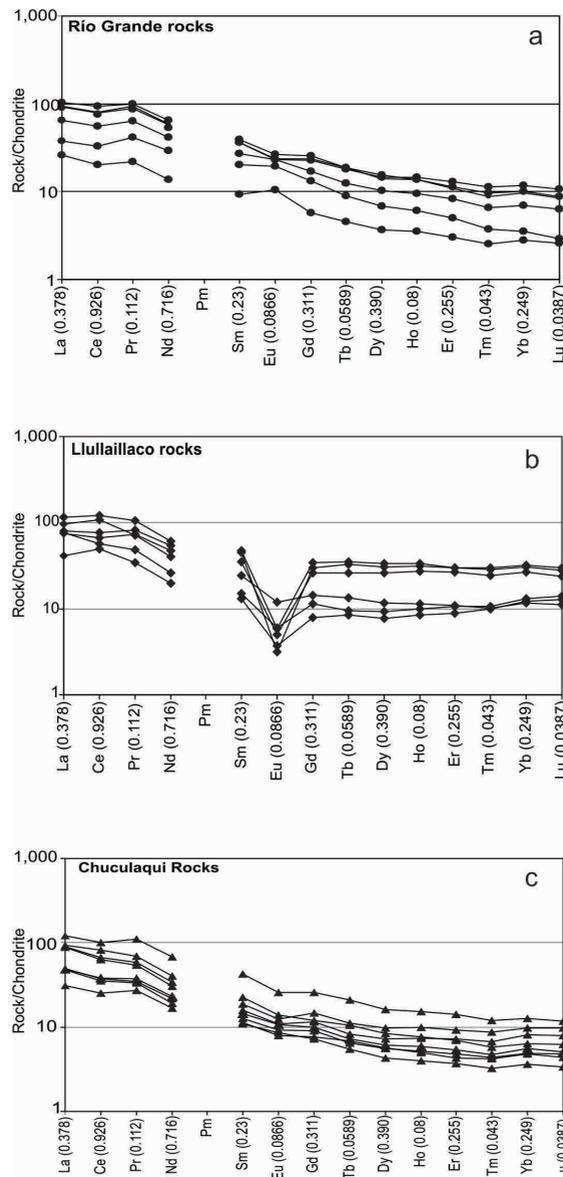
FIG. 4. Leedy chondrite normalized REE concentration patterns (normalizing values from Masuda *et al*., 1973): **a.** Río Grande; **b.** Llullaillaco; **c.** Chuculaqui rock samples. Symbols same as figure 2.

5.1. U-Pb geochronology

Dating young zircons (Phanerozoic) faces the problems of low counts of [207]Pb and the difficulty to detect deviations from slightly older cores and from subtle amounts of Pb loss. To minimize the first problem the time of counting [207]Pb was increased from 10 seconds to 20 seconds, and grains and areas of grains poor in U (<100 ppm) were avoided. Additionally we have used the TuffZirc algorithm (Ludwig and Mundil, 2002), which is largely insensitive to both Pb loss and inheritance to plot the [206]Pb/[238]U ages corrected using the [207]Pb counts. Most of the data group reasonably in the Concordia plots, with few analyses deviating from the Concordia line. All Concordia ages are within error with the TuffZirc ages. These ages are presented as insets in the Concordia plots.
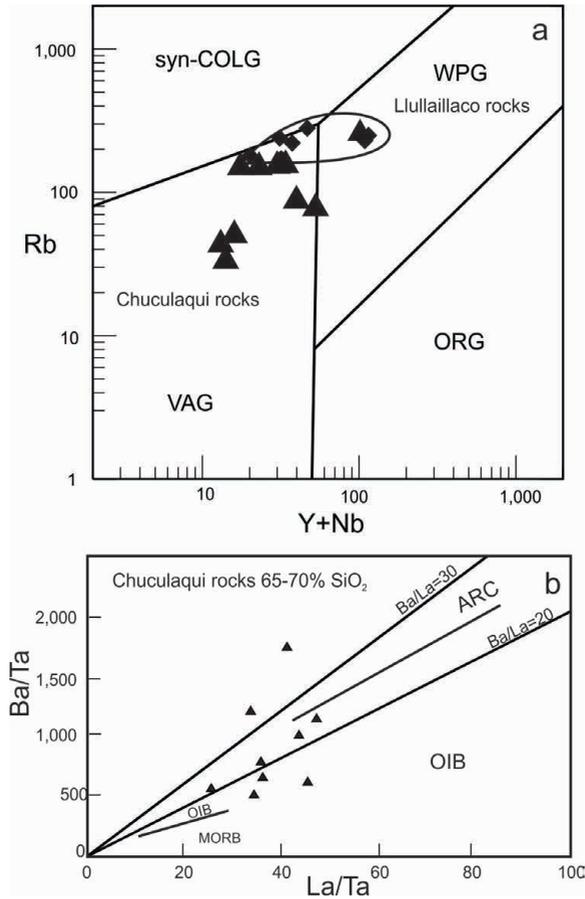
FIG. 5. **a.** Rb *versus* (Y+Nb) discrimination diagram for granites (after Pearce *et al.*, 1984); **b.** Ba/Ta *versus* La/Ta plot based on Gorring and Kay (2001). Symbols same as figure 2.

5.1.1 Río Grande unit

Rocks of this unit are relatively rich in zircon. All grains are 100-300 μm prisms terminated in pyramids (aspect ratio 2:1 to 5:1). The zircon grains are simple and back-scattered electron images show no evidence of older inherited cores or of younger metamorphic rims or zones. They have characteristics of magmatic grains such as the zoning and the Th/U ratios averaging 1.6 (Table 2). Examples of dated zircon are provided in figures 6a to d. Twelve analyses group at the $^{206}Pb/^{238}U$ age of 267±3 Ma (MSWD= 0.019; 2σ) (Fig. 6e). Grains b.2-4 (232±3 Ma), b.5-3 and b.2-1 may be affected by lead loss and are not included in the age calculation. Grain b.5-1 is also not used because its age is highly discordant (-343%). This age is considered the age of crystallization of the gabbro-diorite body.

5.1.2. Llullaillaco Unit

Zircons from sample SA10-03 are short prisms (aspect ratio 2:1 to 3:1), 80 μm to 200 μm long, clear and colorless. Zoning is subtle but present in all grains. Some grains such as b.4-1, g7-1, and g7-3 show recrystallization patches which are brighter (richer in U) in BSE images (Fig. 7a to d). These areas are sealing fractures and represent a later event in the rock. Only one of these patches was analyzed (b.4-1) and effectively yielded the highest U content of 1,807 ppm and the lowest Th/U ratio of the sample (0.05), much lower than the Th/U average of the other zircons (0.68) (cf. Table 2). This patch also has the youngest age of 258±3 Ma (albeit within error with the other ages from this sample). The recrystallization patches may have resulted from the activity of late-magmatic fluids, which may

TABLE 2. U-Pb SHRIMP ISOTOPIC DATA OF ZIRCON FROM THE GONDWANAN MAGMATIC UNITS OF WESTERN PUNA, ARGENTINA.

					Isotopic ratios				Ages		
	U	Th	^{206}Pb	4f^{206}	^{238}U	^{207}Pb	^{207}Pb	^{208}Pb	^{207}Pb	^{206}Pb	Disc.
spot	ppm	U	ppm	(%)	^{206}Pb	^{206}Pb	^{235}U	^{232}Th	^{206}Pb	^{238}U	%
Río Grande, diorite, zircon											
b.1-1	307	1.89	11.2	0.18	23.574±1.49	0.053±3.61	0.308±3.9	0.013±2.35	316±82	268±4	15
b.1-2	150	1.46	5.4	0.27	24.022±1.72	0.053±5.34	0.305±5.61	0.013±2.66	331±121	263±4	21
b.2-1	997	2.15	34.3	0.06	24.962±1.36	0.051±1.46	0.282±2	0.013±1.5	241±34	253±3	-5
b.2-2	402	1.85	14.8	0.16	23.42±1.32	0.050±1.85	0.296±2.28	0.013±1.55	204±43	270±3	-32
b.2-3	90	1.82	3.3	1.34	23.545±2.11	0.054±12.6	0.314±12.7	0.013±4.11	358±284	268±6	25
b.2-4	783	2.04	25.3	0.36	26.687±1.06	0.052±2.6	0.268±2.81	0.012±1.79	283±59	237±2	16
b.3-1	489	1.82	18.1	0	23.143±1.41	0.051±2.02	0.304±2.46	0.014±1.74	238±47	273±4	-15
b.3-2	126	1.98	4.8	0.45	22.589±1.77	0.052±4.81	0.317±5.12	0.014±2.54	279±110	279±5	0
b.4-2	321	1.74	12.2	0.01	22.585±1.56	0.051±3.46	0.312±3.79	0.014±2.1	243±80	279±4	-15
b.4-3	154	1.15	5.4	-0.36	24.375±1.73	0.054±3.31	0.308±3.73	0.013±2.66	389±74	259±4	33
b.4-4	359	1.9	12.8	0.2	24.133±1.47	0.051±2.48	0.289±2.88	0.013±1.84	224±57	262±4	-17
b.5-1	363	1.86	14.1	0.71	22.336±1.63	0.047±5.12	0.292±5.37	0.014±2.23	64±122	282±4	-343
b.5-2	385	1.83	13.7	0	24.122±1.16	0.054±2.14	0.311±2.43	0.013±1.56	391±48	262±3	33
b.5-3	437	1.87	14.9	-0.15	25.086±1.16	0.054±2.15	0.298±2.45	0.012±1.57	379±48	252±3	34
b.6-1	114	0.85	4.2	0.45	23.521±2.3	0.052±5.85	0.305±6.28	0.014±4.16	286±134	268±6	6
b.8-1	313	2.08	11.2	0.31	24.169±1.5	0.050±2.86	0.283±3.23	0.013±1.9	179±67	261±4	-46
Llullaillaco, red granite, zircon											
b.2-1	1,337	0.75	47.7	0.136	24.098±1.37	0.048±2.28	0.274±2.66	0.012±2.01	92±54	262±4	-185
b.3-1	1,650	0.12	58.5	-0.068	24.210±1.34	0.052±1.88	0.297±2.31	0.013±4.12	291±43	261±3	10
b.3-2	732	0.65	26.2	1.298	24.370±1.27	0.053±3.52	0.302±3.74	0.013±4.51	347±80	259±3	25
b.3-3	264	0.84	9.7	2.196	23.961±1.45	0.048±7.42	0.277±7.56	0.012±4.41	103±175	264±4	-156
b.4-1	1,807	0.05	63.5	0	24.451±1.29	0.051±2.07	0.289±2.44	0.014±4.17	253±48	258±3	-2
b.4-2	170	0.82	6.4	0.215	22.678±1.25	0.052±3.37	0.315±3.6	0.013±2.41	275±77	278±3	-1
b.4-3	1,507	0.92	58.3	0.08	22.234±1.08	0.052±1.24	0.320±1.64	0.014±1.44	264±29	284±3	-7
b.5-1	470	0.62	17	0.06	23.769±1.33	0.051±1.93	0.297±2.34	0.013±1.97	248±44	266±3	-7
g.5-1	1,163	0.68	42	0.01	23.782±1.26	0.052±1.44	0.301±1.92	0.013±1.76	282±33	266±3	6
g.5-2	608	0.91	22.8	-0.17	22.863±1.29	0.053±2.66	0.323±2.95	0.014±1.95	349±60	276±3	21
g.6-1	423	0.86	15.3	-0.02	23.676±1.28	0.052±2.04	0.303±2.41	0.014±1.68	288±47	267±3	8
g.7-1	851	0.64	30.3	0.11	24.122±1.31	0.052±2.35	0.295±2.69	0.014±2.07	269±54	262±3	3
g.7-2	1,097	1.03	39.9	0.02	23.639±1.25	0.052±1.26	0.301±1.77	0.014±1.44	266±29	267±3	0
Chuculaqui, granodiorite, zircon											
e.1-1	111	0.66	3.8	0	25.176±1.66	0.053±3,52	0.289±3.89	0.013±3.04	317±80	251±4	21
e.1-2	149	0.68	5	0.13	25.692±1.57	0.053±3,04	0.284±3.42	0.012±2.69	324±69	246±4	24
e.2-1	153	0.68	5.3	0	25.039±1.55	0.052±3,09	0.285±3.46	0.012±2.72	275±71	252±4	8
e.4-1	158	0.84	5.1	0	26.683±1.94	0.052±3.37	0.268±3.89	0.012±2.92	276±77	237±5	14
e.4-2	228	0.85	7.5	0.15	26.329±1.47	0.049±2,53	0.257±2.93	0.012±2.13	155±59	240±3	-55
e.5-1	153	0.85	4.9	0	26.893±1.89	0.052±4,32	0.264±4.72	0.011±3.42	263±99	235±4	11
e.6-1	178	1.16	5.8	0.42	26.489±1.7	0.049±5,74	0.257±5.99	0.011±3.04	164±134	239±4	-46
e.9-1	404	1.27	13	0.23	26.690±1.46	0.051±2,88	0.262±3.23	0.012±2	230±66	237±3	-3

Table 2 continued.

spot	U ppm	Th U	^{206}Pb ppm	$4f^{206}$ (%)	$\frac{^{238}U}{^{206}Pb}$	$\frac{^{207}Pb}{^{206}Pb}$	$\frac{^{207}Pb}{^{235}U}$	$\frac{^{208}Pb}{^{232}Th}$	$\frac{^{207}Pb}{^{206}Pb}$	$\frac{^{206}Pb}{^{238}U}$	Disc. %
					Isotopic ratios				**Ages**		
e.7-1	139	0.64	4.8	0	24.771±1.59	0.051±4.15	0.284±4.44	0.013±2.89	237±96	255±4	-7
e.10-1	213	1.33	7.3	0	25.101±1.55	0.050±2.35	0.275±2.82	0.013±1.98	199±55	252±4	-27
e.11-1	171	0.61	5.7	0.43	25.947±1.69	0.050±5.92	0.263±6.15	0.012±4.47	172±138	244±4	-42
e.12-1	101	0.65	3.4	0	25.370±1.92	0.053±4.49	0.288±4.89	0.012±3.8	329±102	249±5	24
e.13-1	150	1.04	5.1	0.35	25.44±1.72	0.052±6.36	0.279±6.59	0.012±2.94	266±146	249±4	6
Chuculaqui, granodiorite, titanite											
d.2-1	461	0.83	14.9	2.77	27.255±1.73	0.050±5.73	0.252±5.99	0.015±3.18	182±134	232±4	-28
d.3-1	1,049	0.87	34.8	0.85	26.142±1.68	0.053±1.74	0.277±2.42	0.007±2.46	308±40	242±4	21
d.3-2	310	0.85	10.4	3.71	26.543±1.79	0.051±8.08	0.265±8.28	0.021±3.19	243±186	238±4	2
d.3-3	391	0.81	13.4	2.4	25.738±1.72	0.051±5	0.273±5.29	0.020±2.58	235±115	246±4	-5
d.3-4	725	0.84	25.2	1.17	25.004±1.68	0.051±2.32	0.279±2.86	0.008±2.66	222±54	253±4	-14

have occurred shortly after the cooling of the granite (up to 1 or 2 Ma later).

Most of grains (n=10) group at the age of 263±1 Ma (Upper Middle Permian, Capitanian) but a slightly older population of three grains is also present at 280±2 Ma (Lower Permian, Artinskian) (Fig. 7e). The age of 263±1 Ma is considered the age of crystallization of the granitic body that has incorporated components of a slightly older continental crust, probably inherited from intra-arc contamination.

5.1.3. Chuculaqui Unit

U-Pb ages have been determined for zircon and titanite from a granodiorite. The sample has magmatic titanite, which is dark reddish brown occurring as shards of 500-600 µm in diameter (Fig. 8a and b). The mineral is U-rich (average is 631 ppm). The results (Table 2) are concordant. Common lead (*i.e.,* nonradiogenic) is up to 3.71% and average 1.98%. The Concordia age of seven analyses is 247±2 Ma (MSWD=0.76) (Fig. 8e). This titanite is Th-poor and Th/U ratios are almost constant and relatively low (average is 0.85).

The zircon population consists of long prisms 100 to 300 µm long of magmatic origin showing zoning (Fig. 8c and d) and relatively high Th/U ratios (between 0.61 and 1.33). The 13 dated zircons (Table 2) have the same Concordia age at 246±3 Ma (MSWD=1.7).

The age calculated combining the 13 zircons and 7 titanites gives 246±2 Ma (MSWD=0.086, probability=0.77) (Fig. 8f).

The age obtained for the titanite is within uncertainty of the age of the zircons, suggesting that the minerals were co-magmatic.

5.2. Lu-Hf isotopes

While the zircon U-Pb age for igneous rocks represents the timing of magma crystallization, Hf isotopes allow distinguishing juvenile, essentially mantle-derived crust of a given age, having positive $\varepsilon_{Hf(t)}$, from contemporary crust derived from re-melting of older crust, characterized by negative $\varepsilon_{Hf(t)}$. Juvenile magmas are defined as those generated from the depleted mantle or by re-melting of material recently extracted from it (Belousova *et al.*, 2010).

The single-stage Hf model age (T_{DM}) value can be used for zircons with positive $\varepsilon_{Hf(t)}$ as a proxy for the maximum age of magma extraction from the depleted mantle. Otherwise, the two-stage Hf model ($T_{DM(c)}$) provides a first approximation to the source age of host magma from which zircon with negative $\varepsilon_{Hf(t)}$ crystallized. Hf model (T_{DM}) based on a depleted mantle source, is calculated using (^{176}Hf/^{177}Hf) i=0.279718 at 4.56 Ga and ^{176}Lu/^{177}Hf=0.0384, and producing a present-day value of ^{176}Hf/^{177}Hf=0.28325 (Griffin *et al.*, 2000, 2004). The $T_{DM(c)}$ age in zircon is calculated from the initial Hf isotopic composition of the zircon, using an average crustal Lu/Hf ratio (0.015; Griffin *et al.*, 2004). The initial Hf composition of zircon represents the ^{176}Hf/^{177}Hf value calculated at the time
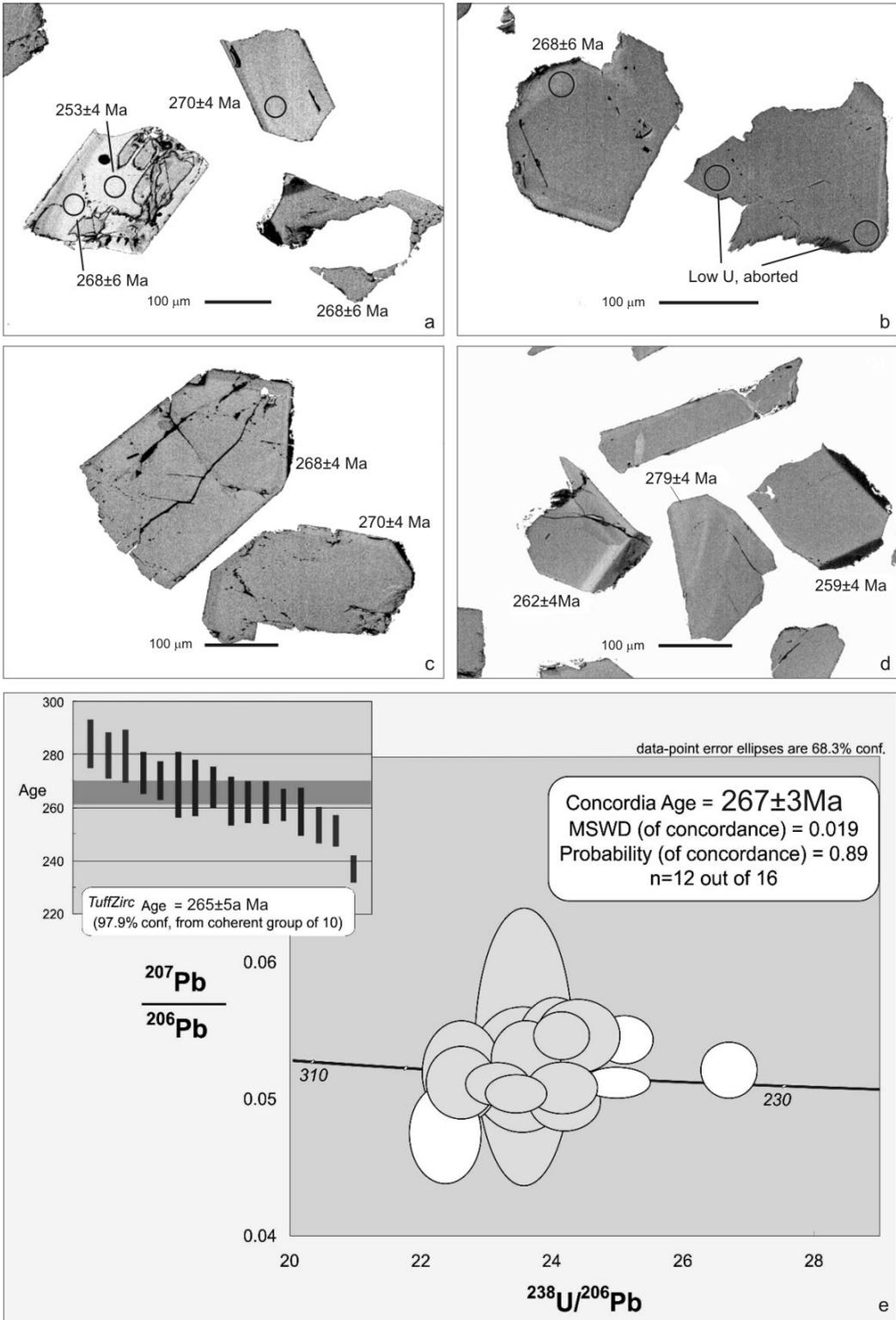
FIG. 6. Examples of dated zircons and concordia diagram for magmatic zircon samples from a Río Grande Unit.
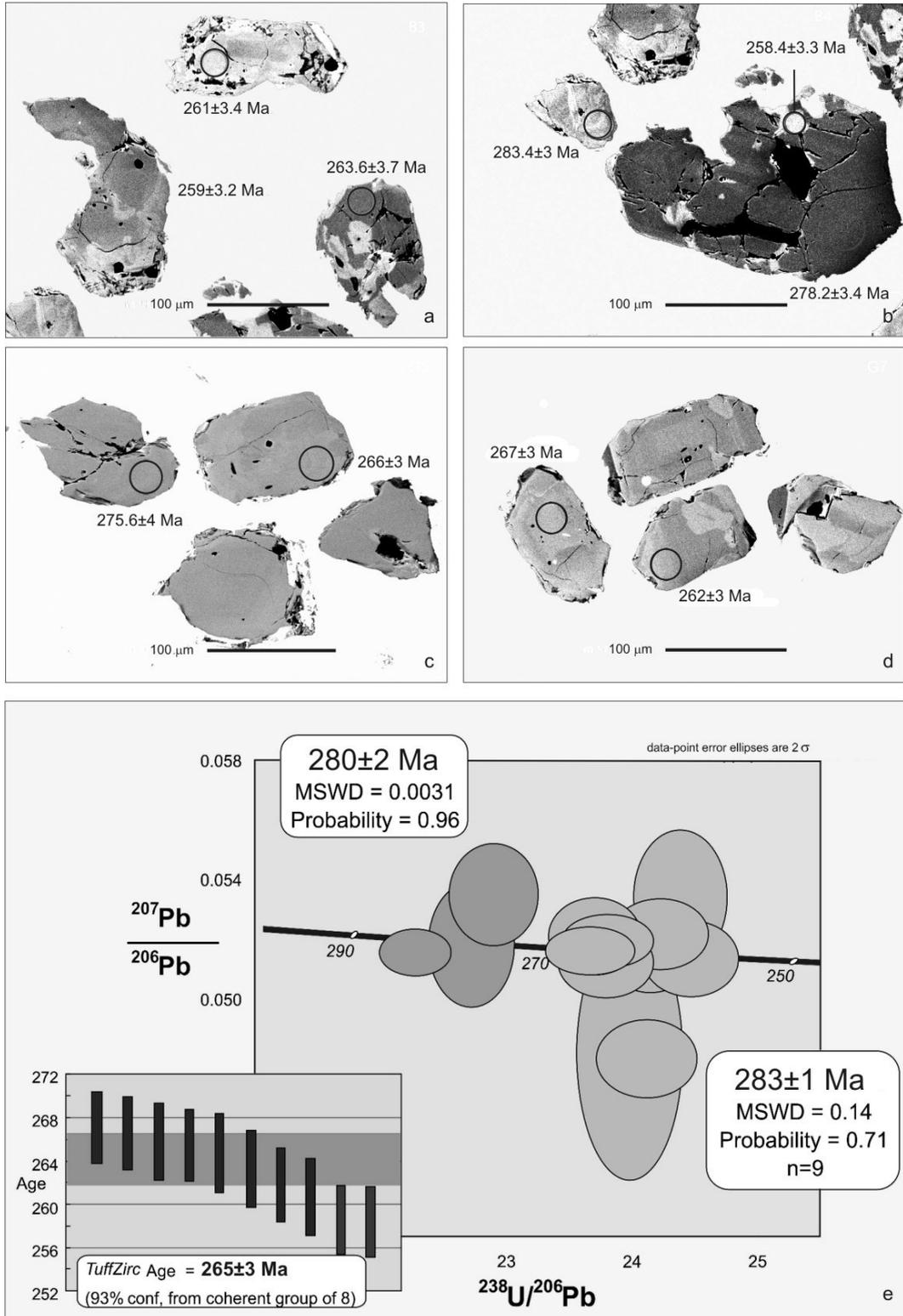
FIG. 7. Examples of dated zircons and concordia diagram for magmatic zircon samples from a Llullaillaco Unit granite.
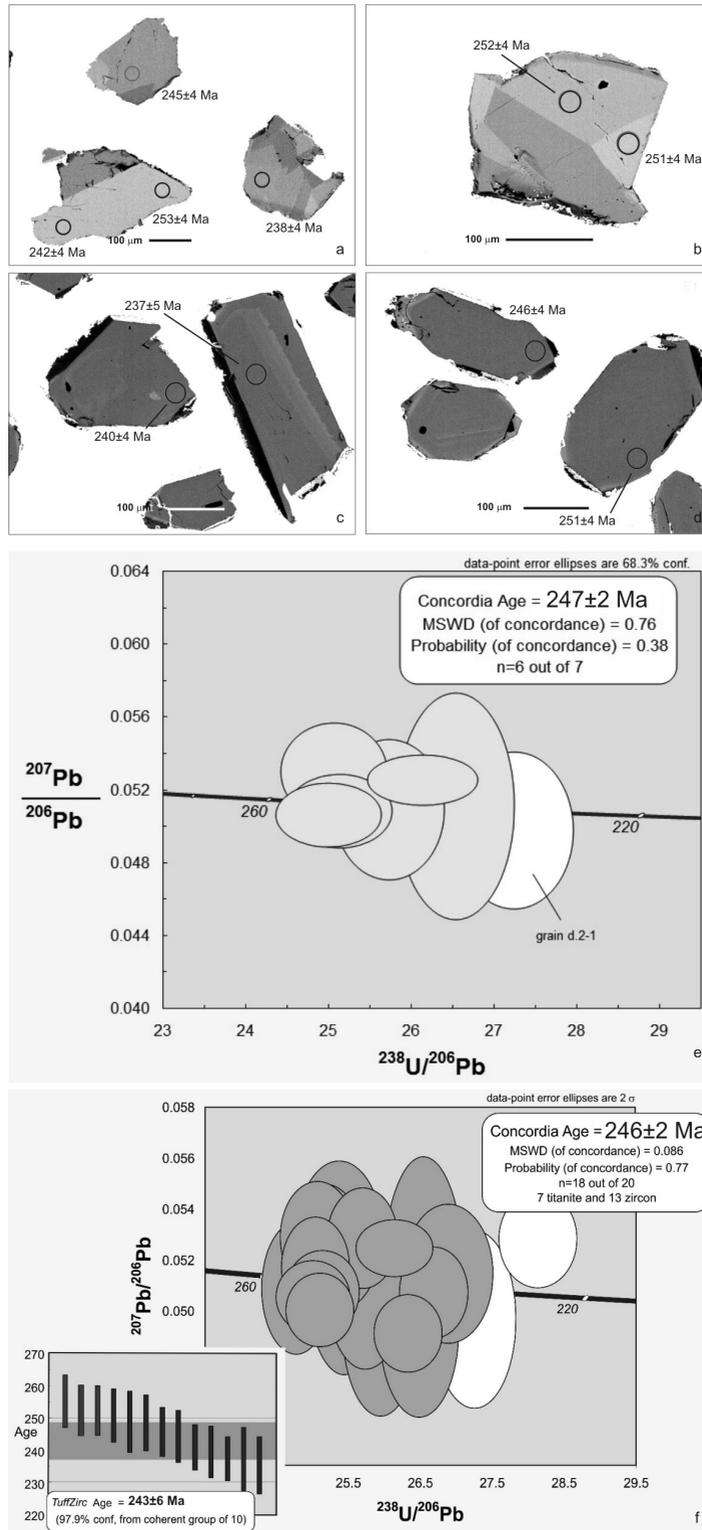
FIG. 8. Examples of dated sphene (**a** and **b**) and zircon (**c** and **d**) samples from a Chuculaqui Unit granodiorite and concordia diagrams for magmatic sphene (**e**) and for combined magmatic sphene and zircon (**f**).

the zircon crystallized, using the U-Pb age previously obtained in the same spot of the same crystal. Such model ages indicate the crustal residence time for the rocks that hosted the zircon.

5.2.1. Río Grande Unit

Eight zircons of the Río Grande unit already dated by U-Pb were selected for Hf analyses. The grains were selected according to the degree of concordance and lower common lead content. All $^{176}Hf/^{177}Hf$ ratios are similar and the data produced negative $\varepsilon_{Hf(t)}$ (from -0.76 to -3.66). The average Lu-Hf model age of the zircon assuming a crustal origin ($T_{DM(c)}$ in table 3) is about 1.4 Ga (Fig. 9a).

5.2.2. Llullaillaco Unit

Ten measurements for Hf isotopes were undertaken on zircons from red granite. The $\varepsilon_{Hf(t)}$ measured in this fraction varies between +1.55 and -3.64, with one outlier at -6.26. This range is mostly coincident with that obtained for Río Grande Formation zircons. The Hf $T_{DM(c)}$ ages obtained range between 1.16 and 1.64 Ga, mostly grouped at 1.24 and 1.36 Ga (Fig. 9b).

5.2.3. Chuculaqui Unit

Hf isotope determinations in the dated Chuculaqui granodiorite zircons all give positive ε_{Hf} values between +1.92 and +5.66 (Fig. 9c). Because of this dominantly juvenile input the values of $\varepsilon_{Hf(t)}$ and Hf model ages were calculated using the one-stage depleted mantle model (Table 3). T_{DM} ages obtained range between 0.65 and 0.79 Ga. These data indicate that the crustal source of the granodiorite has an important juvenile component of Cryogenian age.

6. Discussion and interpretation

6.1. Magma sources

Late Paleozoic-Early Triassic magmatism timing in northern Chile shows two main peaks at about 300 Ma and 244 Ma (Munizaga *et al.*, 2008), with porphyry Cu-Mo type mineralization being related to the younger event. Results obtained in Argentina also show two main episodes of magmatism, with different geochemical and Hf isotope signatures. The younger age obtained (246±2 Ma for Chuculaqui igneous event) is coincident with the younger age reported in Chile, but the older ones (267±3 Ma for the Río Grande, 263±1 Ma for the Llullaillaco

igneous events, as well as the inherited 280±2 Ma zircon population in the latter unit) are not matched by rocks of similar ages in Chile.

When comparing the Hf results for both ages' groups (Fig. 10), the Río Grande and Llullaillaco events have no equivalent in northern Chile, but they share a common Hf evolution trend with the 300 Ma group with more evolved signatures (Cluster 2) suggesting that both magmatic events were sourced by crustal protoliths with similar isotopic signature and Hf model ages. The younger Chuculaqui event has $\varepsilon_{Hf(t)}$ and age values essentially coincident with those of Cluster 3 from Munizaga *et al.* (2008) -which includes the Characolla granite porphyry and El Colorado dacite- both sharing sources with common isotopic imprints.

Hf data obtained from the Río Grande unit suggest the presence of a Mesoproterozoic crust, or sedimentary material derived from such crust, beneath the Puna region. The negative ε_{Hf} also would indicate that these mafic magmas were derived from mantle subsequently contaminated by crustal components.

The $\varepsilon_{Hf(t)}$ variations in the Llullaillaco unit suggest that the melt is derived from a mixed juvenile-crustal source. This range is mostly coincident with that obtained for Río Grande unit zircons, as well as Hf $T_{DM(c)}$ ages that point to a Mesoproterozoic (Sunsás) crust, accordingly suggesting a common origin for both units. The chemistry of high-silica Llullaillaco rocks indicates crustal participation in their parental melts and within-plate extensional affinities.

Otherwise, positive $\varepsilon_{Hf(t)}$ values and T_{DM} ages of about 0.71 Ga in the Chuculaqui unit indicate that the crustal source of the granodiorite has an important juvenile component of Cryogenian age.

From a geochemical point of view the Río Grande unit magmas would appear to have been generated in a setting with intraplate or no-compressional affinities, subsequently contaminated by crustal components as indicted by the Hf isotope data. The lack of inherited xenocrysts should be noted and may result from high magmatic temperatures.

The Llullaillaco granites are representative of a prevailing crustal component without excluding some juvenile mantelic input at the time of magmatism. The dominant crustal source and shallow emplacement are displayed by their geochemical and textural features. The REE pattern is representative of high-silica evolved magmas with LREE depletion caused by minor accessory minerals and

Unit	Analysis No.	^{176}Hf/^{177}Hf	1 σe	^{176}Lu/^{177}Hf	1 σe	U-Pb age (Ma)	^{176}Hf/^{177}Hf initial	epsilon Hf	1 σe	T(DM) (Ga)	T$_{(DM)c}$ crustal
Río Grande	09-36B-Rio G-1.1	0.282591	0.000008	0.0013281	0.000004	267.8	0.2825910	-0.56	0.280	0.91	1.29
Río Grande	09-36B-Rio G-2.1	0.282582	0.000010	0.0018528	0.000050	253.2	0.2825820	-1.29	0.343	0.94	1.33
Río Grande	09-36B-Rio G-2.4	0.282563	0.000011	0.0017236	0.000033	237.1	0.2825630	-2.29	0.385	0.96	1.38
Río Grande	09-36B-Rio G-3.1	0.282579	0.000011	0.0010201	0.000018	272.7	0.2825790	-0.82	0.385	0.92	1.31
Río Grande	09-36B-Rio G-3.2	0.282552	0.000012	0.0018275	0.000069	279.2	0.2825520	-1.79	0.420	0.98	1.38
Río Grande	09-36B-Rio G-4.2.5	0.282537	0.000009	0.0015018	0.000027	279.3	0.2825370	-2.25	0.305	0.99	1.41
Río Grande	09-36B-Rio G-4.4	0.282567	0.000010	0.0019259	0.000013	261.7	0.2825670	-1.65	0.350	0.96	1.36
Río Grande	09-36B-Rio G-6.1.4	0.282504	0.000010	0.0004455	0.000016	268.4	0.2825040	-3.46	0.340	1.01	1.47
Llullaillaco	1126B-02.1	0.282443	0.000034	0.0031847	0.000085	262.1	0.2824268	-6.26	1.190	1.17	1.64
Llullaillaco	1126B-03.1	0.28255	0.000021	0.0039609	0.000160	260.9	0.2825300	-2.63	0.735	1.04	1.42
Llullaillaco	1126B-04.1	0.282515	0.000021	0.0023440	0.000067	258.4	0.2825033	-3.64	0.735	1.05	1.47
Llullaillaco	1126B-04.2	0.282576	0.000009	0.0013394	0.000056	278.2	0.2825688	-0.87	0.301	0.93	1.32
Llullaillaco	1126B-04.3	0.28256	0.000019	0.0028311	0.000140	283.6	0.2825445	-1.60	0.665	1.00	1.37
Llullaillaco	1126B-05.1	0.282561	0.000019	0.0023722	0.000091	265.7	0.2825488	-1.86	0.665	0.98	1.37
Llullaillaco	1138G-05.1	0.282659	0.000016	0.0026880	0.000082	265.5	0.2826452	1.55	0.560	0.85	1.16
Llullaillaco	1138G-06.1	0.282623	0.000009	0.0018223	0.000021	266.7	0.2826136	0.46	0.326	0.88	1.23
Llullaillaco	1138G-07.1	0.282633	0.000017	0.0016833	0.000057	261.9	0.2826245	0.73	0.595	0.86	1.21
Llullaillaco	1138G-07.2	0.282611	0.000019	0.0025071	0.000062	267.1	0.2825980	-0.08	0.665	0.91	1.26
Chuculaqui	09-36E-Chu-1.1.3	0.282696	0.000013	0.0007190	0.000004	251.1	0.2826925	2.89	0.455	0.76	1.07
Chuculaqui	09-36E-Chu-1.2	0.282672	0.000008	0.0007845	0.000019	246.2	0.2826683	1.92	0.287	0.79	1.12
Chuculaqui	09-36E-Chu-2.1.5	0.282726	0.000009	0.0009312	0.000014	252.5	0.2827215	3.95	0.319	0.72	1.00
Chuculaqui	09-36E-Chuc-5.1	0.282762	0.000009	0.0013036	0.000048	235.4	0.2827561	4.78	0.305	0.68	0.94
Chuculaqui	09-36E-Chuc-7.1.3	0.282772	0.000010	0.0009495	0.000011	255.1	0.2827673	5.63	0.350	0.66	0.90
Chuculaqui	09-36E-Chuc-9.1	0.282742	0.000009	0.0009610	0.000018	237.1	0.2827376	4.17	0.312	0.70	0.98
Chuculaqui	09-36E-Chuc-10.1	0.28273	0.000009	0.0008607	0.000005	251.8	0.2827258	4.09	0.312	0.71	1.00
Chuculaqui	09-36E-Chuc-12.1	0.282775	0.000011	0.0006523	0.000008	249.2	0.2827719	5.66	0.385	0.65	0.90
Chuculaqui	09-36E-Chuc-13.1	0.282723	0.000009	0.0004224	0.000008	248.5	0.2827210	3.84	0.322	0.71	1.01

The 'crustal' model ages (T$_{DM (C)}$) assume that the zircon's parental magma was produced from a volume of average continental crust (^{176}Lu/^{177}Hf=0.015; Griffin *et al*., 2004), that was originally derived from the depleted mantle. ^{176}Lu decay is 1.876 x 10-11 yr-1 (Scherer *et al*., 2001).
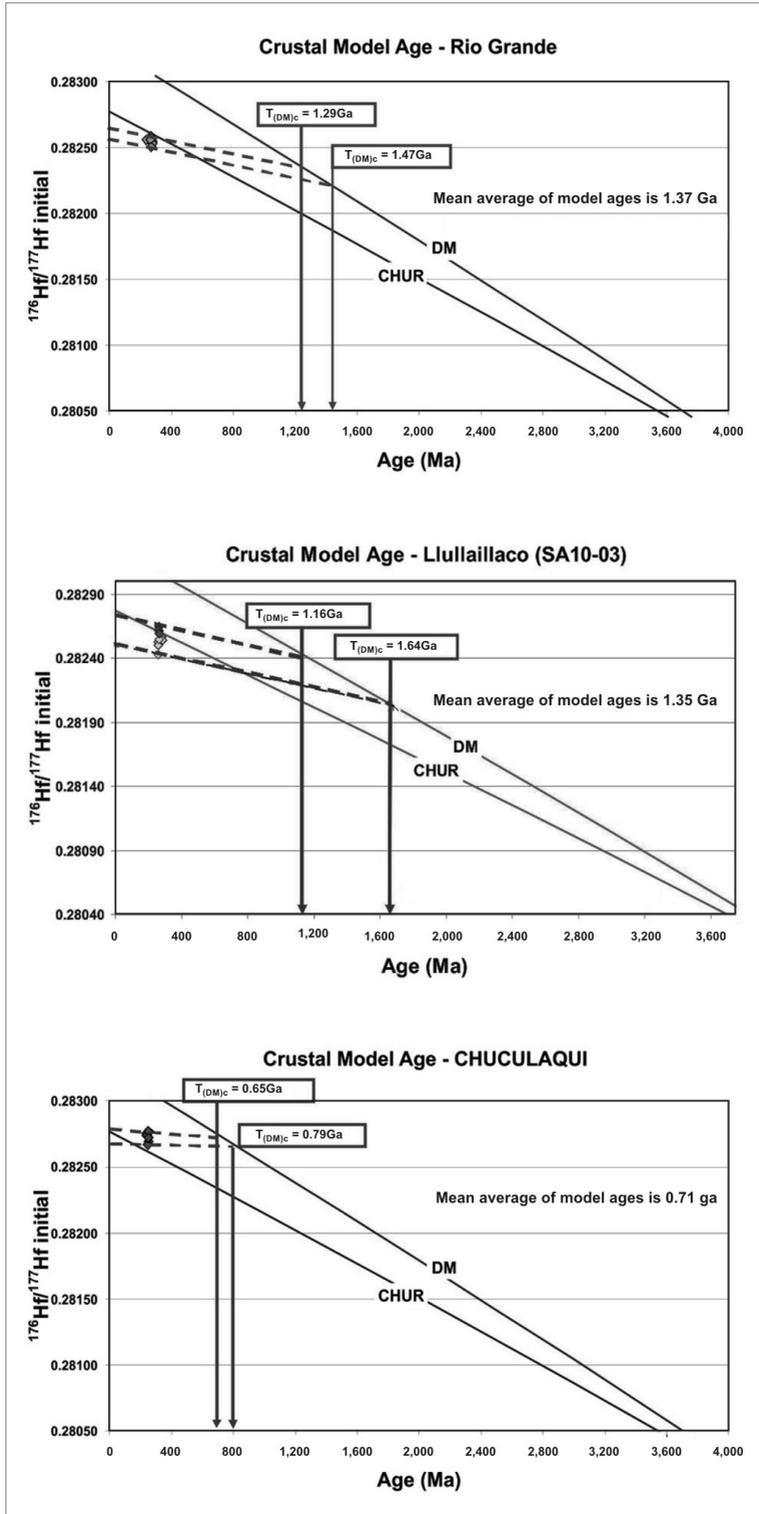
FIG. 9. Diagrams of ^{176}Hf/^{177}Hf (initial) *versus* ^{206}Pb/^{238}U ages of zircons from **a.** the Río Grande Unit diorite; **b.** Llullaillaco Unit granite; and **c.** Chuculaqui Unit granodiorite.
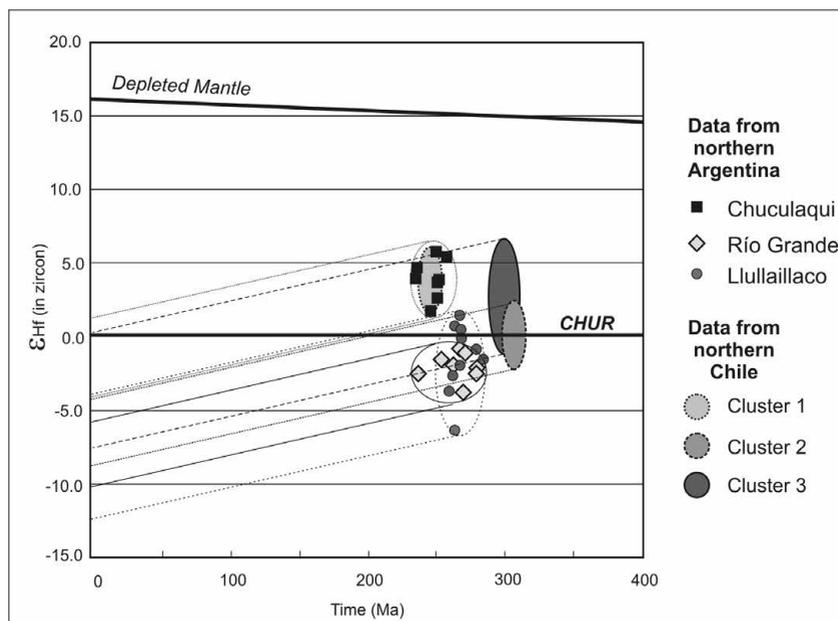
FIG. 10. $\varepsilon_{Hf(T)}$ in zircons *versus* their respective U-Pb age from the Gondwanan magmatic units of Western Puna, Argentina. Fields of data from Munizaga *et al.* (2008) are indicated for comparison.

strong plagioclase fractionation, consistent with the hypersolvus-like features recognized. The negative $\varepsilon_{Hf(t)}$ values obtained as well as the presence of zircon xenocrysts suggest assimilation of older unexposed igneous material, possibly related to the early stages of the same magmatic event evidenced by an older population of zircons of 280±2 Ma with ages coincident to the oldest zircons dated from the Río Grande Unit at 279-282 Ma.

The granitoids of the Chuculaqui unit show typical Cordilleran-type magmatic arc characteristics considering their geochemistry and their evolutionary trend. The positive $\varepsilon_{Hf(t)}$ values for the zircons of this unit also point to relatively juvenile inputs with little presence of recycled crust sources.

The data obtained are consistent with the results presented by Munizaga *et al.* (2008) in Chile, confirming the observation that the magmas show contributions from inhomogeneous older crust material as well as variable magmatic sources, with mixture of crustal melts and mantle-derived magmas.

6.2. The age of the crust in the Puna region: Isotopic constraints

The two stage Depleted Mantle Mesoproterozoic model ages obtained for the Permian Río Grande

and Llullaillaco units indicate a significant residence time in the crust for the magma sources and their emplacement on continental crust. This magmatism in northwest Argentina thus confirms the presence of Mesoproterozoic crustal components mainly Ectasian to Calymnian (1.24 to 1.44 Ga-negative $\varepsilon_{Hf(t)}$) supporting the idea of a continuous basement under the Central Andes, as an extension of the Arequipa-Antofalla massif (Fig. 11). Coincidentally, Zappettini and Santos (2011) have reported Ectasian and Calymnian $T_{DM(c)}$ Hf ages (1.36 and 1.48 Ga) with negative $\varepsilon_{Hf(t)}$ (between 0 and -22.3) from Cretaceous syenitic intrusions in Eastern Puna. Preliminary data obtained by the authors from Ordovician granitoids from Western Puna also point to Calymnian $T_{DM(c)}$ Hf ages (between 1.42 and 1.62 Ga) and negative $\varepsilon_{Hf(t)}$ (between 0 and -3.39).

The $T_{DM(c)}$ Hf ages of zircons at around 1.4 Ga obtained by Munizaga *et al.* (2008) for the Permian magmatism in Chile are also indicative of the presence of the aforementioned Mesoproterozoic (Ectasian to Calymnian) crustal source.

Additionally, the 650 to 790 Ma T_{DM} zircon Hf ages for the Chuculaqui Formation as well as similar data reported by Munizaga *et al.* (2008), with positive $\varepsilon_{Hf(t)}$ and T_{DM} Hf varying between 604 and 748 Ma (recalculated from reported data by Munizaga *et*
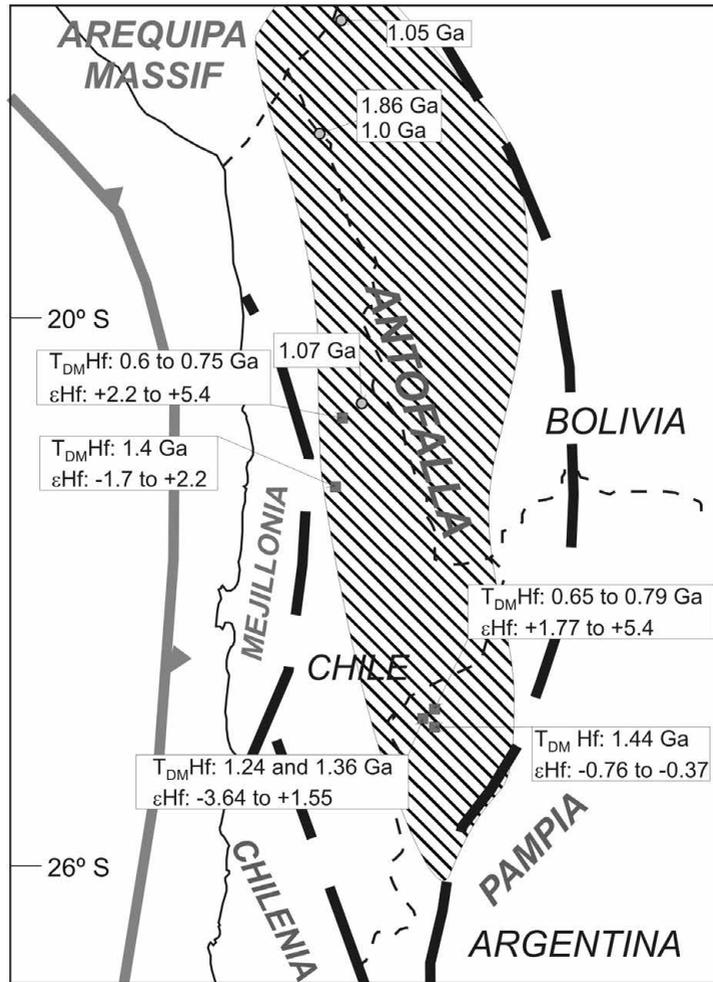
FIG. 11. Main basement blocks with ages from basement outcrops and model ages from the Gondwanan igneous rocks (this paper and
Munizaga *et al*., 2008). Other basement ages from Ramos (2008).

al., 2008) would point to the existence of juvenile, essentially mantle-derived Cryogenian crust in the region, associated with the older Mesoproterozoic basement crust. Similarly, Zappettini and Santos (2011) have reported a 153±2 Ma diorite intrusion in Eastern Puna, with $\varepsilon_{Hf(t)}$ (+2.5 to +5.0) and T_{DM} Hf varying between 620 and 760 Ma. Moreover, the presence of enriched mantle in the 700-800 Ma range (late Rodinia break-up) is already known in Sierras Pampeanas (Rapela *et al.*, 2010) and the data obtained suggest that such enriched mantle was active beneath the Puna region. It should be noted that the Chuculaqui Unit lacks relict or inherited zircon that would point to reworking of ancient crust. This excludes the obtained T_{DM} Hf ages to be interpreted as a binary mix

of such an ancient crust and mantle material at the time of the generation of the granodiorite, although some Triassic juvenile input is not precluded.

The extension of the Arequipa-Antofalla massif beneath the Altiplano, as indicated by the reported Hf data, is consistent with previous Pb-isotopic signature of plutonic rocks from western Puna that confirms the presence of Sunsás-San Ignacio age crust in NW Argentina (cf. Ramos, 2008; Fig. 5 and references therein).

Loewy *et al.* (2004) have defined two domains as constituting the Antofalla basement: the northern one that extends in Chile between Belén and Sierra Moreno includes juvenile magmatism at 1.5-1.4 Ga, evidence of metamorphism at 1.2-1.0 Ga and later

magmatism at about 500-400 Ma; and the southern domain, exposed from Limón Verde in northern Chile to Antofalla in western Argentina Puna (22°-26°S), including juvenile material of 700-600 Ma and magmatism and metamorphism recorded at 500-400 Ma. The studied area pertains to the southern domain, but none of these latter events have been identified, except for the 700 to 600 Ma juvenile magmatic episodes that could be correlated with the 710 Ma T_{DM} zircon Hf ages identified in the Chuculaqui Unit. The 1.24 to 1.36 Ga and 1.0 Ga events would extend the tectonostratigraphic history of this region at least to the Mesoproterozoic and, considering the isolated Statherian $T_{DM(c)}$ Hf age (1.64 Ga) with negative $\varepsilon_{Hf(t)}$, up to the late Paleoproterozoic.

The Arequipa-Antofalla massif is interpreted to be allochthonous to Amazonia (cf. Loewy et al., 2004) and that its accretion to Amazonia would have taken place during the Grenville-Sunsás Orogeny (1.0-1.3 Ga) (Chew et al., 2007). The recorded evidence of Early Mesoproterozoic crust in its southern extension could provide additional evidence for its connection to the Maz and Río Apa blocks, constituting together the hypothetical MARA craton, following the model proposed by Casquet et al. (2009, 2010). The 1.24 to 1.36 Ga crustal ages obtained are coincident with the Andean-type magmatic arc recorded from the Maz terrane at 1.26 to 1.33 Ga (Casquet et al., 2011 and references therein), as well as to the thermal episode at 1.3 Ga that affected the Río Apa block (Cordani et al., 2010), pointing to a common history for the three areas at least during the Mesoproterozoic.

7. Concluding remarks

Gondwanan magmatism developed between Early Carboniferous and Early Triassic times. In NW Argentina it comprises two episodes of different age and genesis: the oldest includes gabbros and diorites (Río Grande Unit) and granitoids (belonging to the Llullaillaco Unit) of late Permian age (Guadalupian) generated in an intraplate environment, hypothetically from an enriched mantle subsequently contaminated with crustal components; the youngest is represented by granodiorites (Chuculaqui Unit) of middle Triassic age (Anisian) with Cordilleran-type arc signature. The results obtained here are comparable to those presented by Munizaga et al. (2008) for northern Chile (see discussion above) and can be related to

the Pre-Andean cycle as distinguished in Chile by Charrier et al. (2007).

The Choiyoi magmatic province, according to Llambías and Sato (1995) and Llambías (1999), developed in a tectonic setting evolving from a late Carboniferous to Permian subduction-related magmatic arc through a collisional regime and subsequent early Triassic post-orogenic granite magmatism, the latter developed in the Argentine side of the Frontal Cordillera. Kleiman and Japas (2009) and Rocha Campos et al. (2011) subdivided the Choiyoi magmatism in a lower section (with ages between 280 and 265 Ma) and an upper section (with ages between 265 and 250 Ma). Triassic volcanic sequences are separately grouped in a synrift phase. Late Triassic to early Jurassic volcanic sequences are grouped further south, in the basement of the Neuquén Basin, into the Precuyano Cycle related also to a rift setting.

We consider that the upper section of the Choiyoi magmatism, with main outcrops in the Frontal Cordillera and San Rafael Block, reaches the NW Argentine Puna where it is represented by the Río Grande and Llullaillaco units. In fact, the tectonic conditions that originated both the Permian magmatism described in this paper and that of the upper section of the Choiyoi series, as well as their geochemical signatures, are analogous. The ages determined in the Puna units are slightly older than those known from further south in the Frontal Cordillera and San Rafael Block (Kleiman and Japas, 2009), suggesting that these common tectonic conditions were originated earlier in the north, with progressive migration to the south.

Conversely, the Triassic magmatism represented by the 246 Ma Chuculaqui Unit in the Puna region cannot be correlated with the upper section of the Choiyoi magmatism from Frontal Cordillera and San Rafael Block, the latter being older than 250 Ma (Rocha Campos et al., 2011). Furthermore, the Triassic magmatism from the Gondwanan Cycle of similar age (246 Ma and younger), identified in the San Rafael Block, has been grouped in the above mentioned synrift phase (Rocha Campos et al., 2011) with geochemical characteristics and tectonic setting emplacement that differ from those identified for the Chuculaqui unit. Rather, the latter could be ascribed to a poorly known continental magmatic arc segment of mostly NS trend. Although during the Pre-Andean tectonic cycle subduction along the

continental margin was presumably interrupted or considerably diminished (Charrier *et al*., 2007) the presence of the Chuculaqui Unit and similar rocks of the same age in northern Chile (Munizaga *et al*., 2008) are indicative of, at least, some restricted subduction related magmatism during the Triassic.

Interestingly, it should be highlighted that in Chile there are porphyry Cu type deposits (La Profunda and Characolla) genetically related to these rocks (Munizaga *et al*., 2008). This implies the presence of an early Triassic metallogenic belt that continues into Argentina, in the areas where the Chuculaqui magmatic event has been defined.

Acknowledgments

References

Alasino, P.H.; Dahlquist, J.A.; Pankhurst, R.J.; Galindo, C.; Casquet, C.; Rapela, C.W.; Larrovere, M.A.; Fanning, C.M. 2012. Early Carboniferous sub- to mid-alkaline magmatism in the Eastern Sierras Pampeanas, NW Argentina: A record of crustal growth by the incorporation of mantle-derived material in an extensional setting. Gondwana Research 22: 992-1008.

Atherton, M.P.; Petford, N. 1990. Géodynamique Andine. Éditions de I'Orstrom: 195-198. Paris.

Bahlburg, H.; Vervoort, J.D.; Du Frane, S.A.; Bock, B.; Augustsson, C.; Reimann, C. 2009. Timing of crust formation and recycling in accretionary orogens: Insights learned from the western margin of South America. Earth-Science Reviews 97 (1): 215-241.

Belousova, E.A.; Kostitsyn, Y.A.; Griffin, W.L.; Begg, G.C.; O'Reilly, S.Y.; Pearson, N.J. 2010. The growth of the continental crust: Constraints from zircon Hf-isotope data. Lithos 119: 457-466.

Bizzarro, M.; Baker, J.A.; Haack, H.; Ulfbeck, D.; Rosing, M. 2003. Early history of Earth's crust-mantle system inferred from hafnium isotopes in chondrites. Nature 421: 931-933.

Bowen, N.L.; Tuttle, O.F. 1950. The system $NaAlSi_3O_8$-$KAlSi_3O_8$-H_2O. Journal of Geology 58: 489-511.

Breitkreuz, C.; Helmdach, F.F.; Kohring, R.; Mosbrugger, V. 1992. Late Carboniferous intra-arc sediments in the north Chilean Andes: stratigraphy, paleogeography and paleoclimate. Facies 26 (1): 67-80.

Breitkreuz, C.; Van Schmus, W.R. 1996. U-Pb geochronology and significance of Late Permian ignimbrites in Northern Chile. Journal of South American Earth Sciences 9 (5-6): 281-293.

Breitkreuz, C.; Zeil, W. 1994. Geodynamic and magmatic stages on a traverse through the Andes between 20° and 24°S (N Chile, SW Bolivia, NW Argentina). Journal of Geological Society of London 141: 861-868.

Brown, M. 1991. Comparative geochemical interpretation of Permian-Triassic plutonic complexes of the Coastal Range and Altiplano (25ª30' to 26ª30'S), northern Chile. *In* Andean magmatism and its tectonic setting (Harmon, R.S.; Rapela, C.W.; editors). Geological Society of America, Special Paper 265: 157-177. Boulder, Colorado.

Casquet, C.; Rapela, C.W.; Pankhurst, R.J.; Baldo, E.; Galindo, C.; Fanning, M.; Saavedra, J. 2009. Proterozoic terranes in southern South America: accretion to Amazonia, involvement in Rodinia fonnation and fiuther west Gondwana accretion. *In* Rodinia: Supercontinents, Superplumes and Scotland. Geological Society of London, Fennor Meeting, Edinburgh, Abstract: p. 61.

Casquet, C.; Rapela, C.W.; Pankhurst, R.J.; Baldo, E.; Galindo, C.; Fanning, M.; Dahlquist, J.A.; Saavedra, J. 2010. A history of Proterozoic terranes in southern South America: From Rodinia to Gondwana. Geoscience Frontiers 3 (2): 137-145.

Casquet, C.; Rapela, C.W.; Pankhurst, R.J.; Baldo, E.G.; Galindo, C.; Fanning, C.M.; Dahlquist, J.A.; Saavedra, J. 2011. A history of Proterozoic terranes in southern South America: From Rodinia to Gondwana. Geoscience Frontiers 3 (2): 137-145.

Charrier, R.; Pinto, L.; Rodríguez, M.P. 2007. Tectonostratigraphic evolution of the Andean Orogen in Chile. *In* The Geology of Chile (Moreno, T.; Gibbons, W.; editors). The Geological Society: 21-114.

Chew, D.; Schaltegger, U.; Kosler, J.; Whitehouse, M.J.; Gutjahr, M.; Spikings, R.A.; Mišković, A. 2007. U-Pb geochronologic evidence for the evolution of the Gondwanan margin of the north-central Andes. Geological Society of America Bulletin 119: 697-711.

Coira, B. 2008. Volcanismo del Paleozoico Inferior en la Puna Jujeña. *In* Geología y Recursos Naturales de la Provincia de Jujuy (Coira, B; Zappettini, E; editors).

In Congreso Geológico Argentino, No. 17, Relatorio: 140-154. Buenos Aires.

Cordani, U.G.; Teixeira, W.; Tassinari, E.G.; Coutinho, J.M.V.; Ruiz, A.S. 2010. The Río Apa craton in Mato Grosso do Sul (Brazil) and northern Paraguay: geochronological evolution, correlations and tectonic implications for Rodinia and Gondwana. American Journal of Science 310: 981-1023.

Cox, K.G.; Bell, J.D.; Pankhurst, R.J. 1979. The interpretation of igneous rocks. George Allen and Unwin: 450 p. London.

Gardeweg, M.; Ramírez, C.; Davidson, J. 1993. Mapa geológico del área del salar de Punta Negra y del volcán Llullaillaco. Región de Antofagasta. Servicio Nacional de Geología y Minería, Documentos de trabajo 5. 1 mapa escala 1:100.000. Santiago.

Gorring, M.L.; Kay, S.M. 2001. Mantle Processes and Sources of Neogene Slab Window Magmas from Southern Patagonia, Argentina. Journal of Petrology 42 (6): 1067-1094.

Griffin, W.L.; Pearson, N.J.; Belousova, E.A.; Jackson, S.R.; van Achterbergh, E.; O'Reilly, S.Y.; Shee, S.R. 2000. The Hf isotope composition of cratonic mantle: LAM-MC-ICPMS analysis of zircon megacrysts in kimberlites. Geochimica et Cosmochimica, Acta 64: 133-147.

Griffin, W.L.; Belousova, E.A.; Shee, S.R.; Pearson, N.J.; O'Reilly, S.Y. 2004. Archean crustal evolution in the northern Yilgarn Craton: U-Pb and Hf-isotope evidence from detrital zircons. Precambrian Research 131: 231-282.

Groeber, P. 1946. Observaciones geológicas a lo largo del meridiano 70°1, Hoja Chos Malal. Revista de la Sociedad Geológica Argentina 1 (3): 117-208.

Groeber, P. 1951. La Alta Cordillera entre las latitudes 34° y 29°30'. Instituto de Investigaciones de las Ciencias Naturales. Museo Argentino de Ciencias Naturales Bernardino Rivadavia, Ciencias Geológicas 1 (5): 1-352. Buenos Aires.

Kay, S.M.; Ramos, V.A.; Mpodozis, C.; Sruoga, P. 1989. Late Paleozoic to Jurassic silicic magmatism at the Gondwanaland margin: analogy to the Middle Proterozoic in North America? Geology 17: 324-328.

Kleiman, L.E.; Japas, M.S. 2009. The Choiyoi volcanic province at 34°-36°S (San Rafael, Mendoza, Argentina): implications for the late Paleozoic evolution of the southwestern margin of Gondwana. Tectonophysics 473: 283-299.

Kontak, D.J.; Clark, A.H.; Farrar, E.; Archibald, D.A.; Baadsgaard, H. 1990. Late Paleozoic-early Mesozoic magmatism in the Cordillera de Carabaya, Puno, southeastern Perú: Geochronology and petrochemistry. Journal of South American Earth Sciences 3 (4): 213-230.

Llambías, E.J. 1999. Las rocas ígneas gondwánicas. 1. El magmatismo gondwánico durante el Paleozoico superior-Triásico. *In* Geología Argentina. Instituto de Geología y Recursos Minerales, Servicio Geológico Minero Argentino, Anales 29 (14): 349-376. Buenos Aires.

Llambías, E.J.; Sato, A.M. 1990. El Batolito de Colangüil, Cordillera Frontal, Argentina: Estructura y marco tectónico. Revista Geológica de Chile 17 (1): 89-108.

Llambías, E.J.; Sato, A.M. 1995. El batolito de Colangüil: transición entre orogénesis y anorogénesis. Revista de la Asociación Geológica Argentina 50 (1-4): 111-131.

Llambías, E.J.; Kleiman, L.E.; Salvarredi, J.A. 1993. El magmatismo gondwánico. *In* Congreso Geológico Argentino, No. 12 y Congreso de Exploración de Hidrocarburos, No. 2. Geología y Recursos Naturales de Mendoza (Ramos, V.A; editor), Relatorio 1: 53-64. Mendoza.

Loewy, S.L.; Connelly, J.N.; Dalziel, I.W.D. 2004. An orphaned basement block. The Arequipa-Antofalla basement of the central Andean margin of South America. Geological Society of America Bulletin 116: 171-187.

Lucassen, F.; Franz, G.; Thirlwall, M.F.; Mezger, K. 1999. Crustal recycling of metamorphic basement, Late Paleozoic granitoids of northern Chile (~22°S): implications for the composition of the Andean crust. Journal of Petrology 40: 1527-1551.

Ludwig, K.R. 2001. Squid 1.02: A Users Manual. Berkeley Geochronology Centre, Special Publication 2: 19 p.

Ludwig, K.R. 2003. Isoplot 3.00. A Geochronological Tool-kit for Excel. Berkeley Geochronology Center, Special Publication 4: 67 p.

Ludwig, K.R.; Mundil, R. 2002. Extracting reliable U-Pb ages and errors from complex populations of zircons from Phanerozoic tuffs. Goldschmidt Conference Abstracts A463: 908 p. Davos Switzerland.

Masuda, A.; Nakamura, N.; Tanaka, T. 1973. Fine structures of mutually normalised rare earth patterns of chondrites. Geochimica et Cosmochimica, Acta 37: 239-248.

Mišković, A.; Spikings, R.A.; Chew, D.M.; Košler, J.; Ulianov, A.; Schaltegger, U. 2009. Tectonomagmatic evolution of Western Amazonia: Geochemical characterization and zircon U-Pb geochronologic constraints from the Perúvian Eastern Cordilleran granitoids. Geological Society of America Bulletin 121 (9-10): 1298-1324.

Mpodozis, C.; Ramos, V.A. 1990. The Andes of Chile and Argentina. *In* Geology of the Andes and its relation to Hydrocarbon and Mineral Resources (Ericksen, G.E.; Cañas-Pinochet, M.T.; Reinemud, J.A.; editors). Circumpacific Council for Energy and Mineral Resources, Earth Sciences Series 11: 59-90. Houston.

Mpodozis, C.; Kay, S. 1992. Late Paleozoic to Triassic evolution of the Gondwana margin: Evidence from Chilean Frontal Cordillera batholiths (28°S to 31°S). Geological Society of America Bulletin 104: 999-1014.

Munizaga, F.; Maksaev, V.; Fanning, C.M.; Giglio, S.; Yaxley, G.; Tassinari, C.C.G. 2008. Late Paleozoic-Early Triassic magmatism on the western margin of Gondwana: Collahuasi area, Northern Chile. Gondwana Research 13: 407-427.

Naranjo, J.; Cornejo, P. 1992. Mapa Geológico Salar de la Isla. Servicio Nacional de Geología y Minería. Serie Geología Básica 72. 1 mapa escala 1:250.000. Santiago.

Omarini, R.H.; Sureda, R.J.; López de Azarevich, V.; Hauser, N. 2008. El Basamento Neoproterozoico Cámbrico inferior en la Provincia de Jujuy. *In* Congreso Geológico Argentino, No. 17, Geología y Recursos Naturales de la Provincia de Jujuy (Coira, B.; Zappettini, E.O.; editors), Relatorio: 17-28. Buenos Aires.

Page, S.; Zappettini, E. 1999. Magmatismo, provincias de Jujuy, Salta, Tucumán y Catamarca. *In* Congreso Geológico Argentino, No. 14. Geología del Noroeste Argentino (González-Bonorino, G.; Omarini, R.; Viramonte, J.; editors), Relatorio: 241-253. Salta.

Pankhurst, R.J.; Rapela, C.W.; Saavedra, J.; Baldo, E.; Dahlquist, J.; Pascua, I.; Fanning, C.M. 1998. The Famatinian magmatic arc in the central Sierras Pampeanas: an Early to Mid-Ordovician continental arc on the Gondwana margin. *In* The Proto-Andean Margin of Gondwana, No. 142 (Pankhurst, R.J.; Rapela, C.W.; editors). Geological Society of London, Special Publications: 343-368.

Pearce, J. 1983. Role of the sub-continental lithosphere in magma genesis at active continental margins. *In* Continental basalts and mantle xenoliths (Hawkesworth, C.J.; Norry, M.J.; editors). Shiva Publishing: 230-249. Nantwich.

Pearce, J.A.; Harris, N.B.W.; Tindle, A.G. 1984. Trace Element Discrimination Diagrams for the Tectonic Interpretation of Granitic Rocks. Journal of Petrology 25 (4): 956-983.

Peccerillo, R.; Taylor, S.R. 1976. Geochemistry of Eocene calc-alkaline volcanic rocks from the Kastamonu area, Northern Turkey. Contributions to Mineralogy and Petrology 58: 63-81.

Poma, S.; Quenardelle, S.; Koukharsky, M. 2009. Puna granitic plutonism as possible Northern continuation of the Late Paleozoic-Early Triassic magmatic arc from the Frontal Cordillera, Argentina. *In* Geological Society of America Annual Meeting. Abstracts with Programs 41 (7): 113 p. Portland.

Poma, S.; Quenardelle, S.; Litvak, V.; Maisonnave, E.B.; Koukharsky, M. 2004. The Sierra de Macon, Plutonic expression of the Ordovician magmatic arc, Salta Province Argentina. Journal of South American Earth Sciences 16: 587-597.

Ramírez, C.; Gardeweg, M.; Davidson, J.; Pino, H. 1991. Mapa geológico del área de los volcanes Socompa y Pular, Región de Antofagasta. Servicio Nacional de Geología y Minería. Documentos de trabajo 4. 1 mapa escala 1:100.000. Santiago.

Ramos, V.A. 2008. The basement of the Central Andes: The Arequipa and related terranes. Annual Review of Earth and Planetary Sciences 36: 289-324.

Ramos, V.A.; Vujovich, G.; Martino, R.; Otamendi, J. 2010. Pampia: a large cratonic block missing in the Rodinia supercontinent. Journal of Geodynamics 50: 243-255.

Rapela, C.W.; Pankhurst, R.J.; Casquet, C.; Baldo, E.; Saavedra, J.; Galindo, C.; Fanning, C.M. 1998. The Pampean orogeny of the southern proto-Andes: evidence for Cambrian continental collision in the Sierras de Cordoba *In* The Proto-Andean Margin of Gondwana, No. 142 (Pankhurst, R.J.; Rapela, C.W.; editors). Geological Society of London, Special Publications: 181-217.

Rapela, C.W.; Pankhurst, R.J.; Casquet, C.; Baldo, E.; Galindo, C.; Fanning, C.M.; Dahlquist, J.M. 2010. The Western Sierras Pampeanas: Protracted Grenville-age history (1330-1030 Ma) of intra-oceanic arcs, subduction-accretion at continental-edge and AMCG intraplate magmatism. Journal of South American Earth Sciences 29: 105-127.

Rocha-Campos, A.C.; Basei, M.A.; Nutman, A.P.; Kleiman, L.E.; Varela, R.; Llambías, E.; Canile, F.M.; da Rosa, O.; de, C.R. 2011. 30 million years of Permian volcanism recorded in the Choiyoi igneous province (W Argentina) and their source for younger ash fall deposits in the Paraná Basin: SHRIMP U-Pb zircon geochronology evidence. Gondwana Research 19: 509-523.

Rolleri, E.O.; Criado-Roque, P. 1970. Geología de la provincia de Mendoza. *In* Jornadas Geológicas Argentinas, No. 4 (1969). Asociación Geológica Argentina, Actas 2: 1-60. Buenos Aires.

Scherer, E.; Munker, C.; Mezger, K. 2001. Calibration of the Lutetium-Hafnium clock. Science 293: 683-687.

Taylor, S.R.; McLennan, S.M. 1995. The geochemical evolution of the continental crust. Reviews in Geophysics 33: 241-265.

Tuttle, O.F.; Bowen, N.L. 1958. Origin of granite in the light of experimental studies in the system the system $NaAlSi_3O_8$-$KAlSi_3O_8$-SiO_2-H_2O. Geological Society of America Memoir 74: 153 p.

Willner, A.P.; Massonne, H.J.; Gerdes, A.; Hervé, F.; Sudo, M.; Thomson, S. 2009. The contrasting evolution of collisional and coastal accretionary systems between the latitudes 30º and 35ºS: evidence for the existence of a Chilenia microplate. *In* Congreso Geológico Chileno, No. 12 (S9_099): p 4. Santiago.

Zappettini, E.O. 2008. Plutonismo Paleozoico Inferior de la Puna Oriental. *In* Geología y Recursos Naturales de la Provincia de Jujuy (Coira, B.; Zappettini, E.O.; editors). *In* Congreso Geológico Argentino, No. 17, Relatorio: 642 p. Buenos Aires.

Zappettini, E.O.; Blasco, G. 1998. Hoja Geológica 2569-II Socompa, provincia de Salta. Servicio Geológico Minero Argentino (SEGEMAR), Boletín 160: 83 p. Buenos Aires.

Zappettini, E.O.L.; Santos, J.O. 2011. El plutonismo alcalino de intraplaca mesozoico en la Puna argentina: Edades U-Pb SHRIMP en circones, determinaciones isotópicas de Hafnio e implicancias geodinámicas. *In* Congreso Geológico Argentino, No. 18, Actas DVD-Rom. Neuquén.

Appendix

Description of methods

Representative samples of the three units were analyzed for major elements by inductively coupled plasma (ICP) and for trace and rare earth elements by ICP Mass Spectrometry (ICP-MS) at Activation Laboratories of Ancaster, Ontario, Canada. Representative data from main group types are presented in table 1.

U-Pb analysis of zircon was carried out at Curtin University of Technology, Perth. Samples RG (diorite from Río Grande Unit), CHUQ (granodiorite from Chuculaqui Unit) and SA10-03 (red granite from Llullaillaco Unit) have been crushed, milled, sieved, and washed to remove very fine material (clay and silt sizes). The 60-250 mesh fractions were treated with heavy liquids (to remove light minerals) and magnetic separator (to concentrate the less magnetic minerals such as zircon). Zircon was handpicked and organized in an epoxy mount, which was polished and carbon-coated for SEM (Scanning Electron Microscope) study. Back-scattered images (BSE) were taken using a JEOL6400 SEM at the Centre for Microscopy and Microanalyses at University of Western Australia. Images of zircon are critical for identifying internal features such as core and rims and to help avoiding areas with high common lead content (inclusions, fractures, and metamict areas). Epoxy mount (UWA 05-85) was gold-coated for SHRIMP analyses.

Sensitive High Mass Resolution Ion MicroProbe (SHRIMP II) U-Pb analyses were performed at Curtin University, under a Consortium between that university, the Western Australia University, and the Geological Survey of Western Australia. Data was collected in two sessions using an analytical spot size of about 20-25 mm. Individual analyses are composed of measurement of nine masses repeated in five scans. The following masses were analyzed for zircon: (Zr_2O, ^{204}Pb, background, ^{206}Pb, ^{207}Pb, ^{208}Pb, ^{238}U, ^{248}ThO, ^{254}UO). The standards D23 and NBS611 were used to identify the position of the peak of the mass ^{204}Pb, whereas the calibration of the U-content and the Pb/U ratio were done using the zircon standard BR266 (559 Ma, 903 ppm U). Data were reduced using the SQUID© 1.03 software (Ludwig, 2001) and the ages calculated using Isoplot© 3.0 (Ludwig, 2003). The Phanerozoic ages are mean average $^{206}Pb/^{238}U$ ages where the common lead is corrected using the 207Pb content. The uncertainties of individual ages are quoted at 1σ whereas the final ages and those used in the plots are calculated at 2σ level (about 95% confidence).

Hf-isotope analyses reported here were carried out in situ using a New Wave Research LUV213 laser-ablation microprobe, attached to a Nu Plasma multicollector ICPMS at GEMOC Key Centre, Macquarie University, Sydney. Most analyses are carried out with a beam diameter of about 40 μm, a 10 Hz repetition rate, and energies of 0.6-1.3 mJ/pulse. Typical ablation times are 30-120 s, resulting in pits 20-40 μm deep. The analytical spots of Hf-isotope analyses were located in the same site of the previous U-Pb SHRIMP analyses. Isobaric interferences of ^{176}Lu and ^{176}Yb on ^{176}Hf were corrected by the Nu Plasma because the mass bias of the instrument is independent of mass over the mass range considered. Interference of ^{176}Lu on ^{176}Hf is corrected by measuring the intensity of the interference-free ^{175}Lu isotope and using $^{176}Lu/^{175}Lu=0.02669$ to calculate the intensity of ^{176}Lu. Similarly, the interference of ^{176}Yb on ^{176}Hf is corrected by measuring the interference-free ^{172}Yb isotope and using $^{176}Yb/^{172}Yb$ to calculate the intensity of ^{176}Yb. The spiking of JMC475 Hf standard is used to determine the value of $^{176}Yb/^{172}Yb$ (0.5865) required to yield the value of $^{176}Hf/^{177}Hf$ obtained on the pure Hf solution.

The ^{176}Lu decay constant used to calculate initial $^{176}Hf/^{177}Hf$, ε_{Hf} values, and model age is $1.983 \times 10-11$ (Bizzaro *et al*., 2003). Typical uncertainties on single $^{176}Lu/^{177}Hf$ analyses are about 1 sigma unit (±0.001-0.002%) incorporating both spatial variation of Lu/Hf and analytical uncertainties. Chondritic values of Scherer *et al*. (2001) (1.865x10-11) have been used for the calculation of ε_{Hf} values. A model of ($^{176}Hf/^{177}Hf$) i= 0.279718 at 4.56 Ga and $^{176}Lu/^{177}Hf$ = 0.0384 has been used to calculate model ages (T_{DM}) based on a depleted mantle source, producing a present-day value of $^{176}Hf/^{177}Hf$ (0.28325) (Griffin *et al*., 2000, 2004). T_{DM} ages, which are calculated using measured $^{176}Hf/^{177}Hf$ of the zircon, give only the minimum age for the source material from which the zircon crystallized. We have also calculated a 'crustal' model age ($T_{DM(c)}$) for each zircon which assumes that the parental magma was produced from an average continental crust ($^{176}Lu/^{177}Hf$ = 0.015) (Griffin *et al*., 2004) that was originally derived from depleted mantle.

Hf data are given in table 3. ε_{Hf} values, also summarized in table 3, were calculated at the $^{206}Pb/^{238}U$ age of each grain (T).